Streptococcus pneumoniae with biosynthesis gene mutations attenuate disease but retain their potential for epithelial microinvasion and epithelial innate immune activation

Short title: Pneumococcal epithelial microinvasion and induction of innate immunity

Caroline M. Weight[1*], Gabriele Pollara[1], Modupeh Betts[1], Roberta Ragazzini[2], Michael Connor[3], Elisa Ramos-Sevillano[4], Jesús Reiné[5], Matthew Whelan[1], José Afonso Guerra-Assunção[1], Paola Bonfanti[1,2], Clare Jolly[1], Mahdad Noursadeghi[1], Daniela M. Ferreira[5], Jeremy S. Brown[4], Robert S. Heyderman[1]

[1]Research Department of Infection, Division of Infection and Immunity, UCL London, UK

[2]Francis Crick Institute, London, UK

[3]Chromatin and Infection, Institut Pasteur, France

[4]Department of Respiratory Medicine, UCL, London, UK

[5]Oxford Vaccine Group, University of Oxford, Oxford and Clinical Sciences, Liverpool School of Tropical Medicine, Liverpool, UK

*Current address Biomedical and Life Sciences, Faculty of Health and Medicine, Lancaster University, UK

Corresponding Authors: Dr Caroline M. Weight and Professor Robert S. Heyderman

Email: c.weight@lancaster.ac.uk and r.heyderman@ucl.ac.uk

ABSTRACT

Colonisation of the nasopharynx by *Streptococcus pneumoniae* is characterised by adherence to epithelial cells, microinvasion and an innate immune response. Here, we explore the hypothesis that pneumococcal virulence has primarily evolved to promote these colonisation processes and subsequent transmission, rather than to cause disease. We have used a *S. pneumoniae* serotype 6B strain, alongside two biosynthesis gene mutants (Δ*proABC* and Δ*fhs* with an additional Δ*piaA* mutation) known to colonise murine and human models without causing disease. We show that these *S. pneumoniae* mutations do not attenuate microinvasion in either experimental human pneumococcal challenge (EHPC) or *in vitro* in primary and immortalised epithelial cells. Additionally, we show that *S. pneumoniae* infection of primary human airway epithelium triggers strain-dependent cellular reorganisation, with preserved barrier function. The pro-inflammatory epithelial innate response and caspase 8 activity associated with these processes are attenuated by the Δ*fhs/piaA* but not the Δ*proABC/piaA* mutation. Compared to the WT and Δ*proABC/piaA* mutant strains, growth of the Δ*fhs/piaA* mutant was associated with increased pneumococcal hydrogen peroxide secretion and reduced pneumolysin activity. Analysis of the bacterial transcriptome under stress conditions revealed that deletion of the *proABC* and *fhs* genes had broad, differential effects on pneumococcal virulence and metabolic gene expression suggestive of compensatory changes that preserve microinvasion. The findings that cellular reorganisation, the innate immune response, and the ability to cause invasive disease are not necessarily interconnected emphasise the complexity of bacterial-host interactions at the mucosal surface. The outcome of colonisation at this crucial barrier cannot be fully explained by single or functionally grouped virulence or metabolic factors.

INTRODUCTION

Adaptation to the host environment is crucial for successful colonisation of the upper respiratory tract (URT) by a range of human pathogens, including bacteria, viruses and fungi. This includes the ability to withstand different ambient temperatures, overcome physical barriers such as mucus, evade epithelial soluble mediators such as antimicrobial peptides, compete with neighbouring polymicrobial communities and compensate for nutrient restriction (1). *Streptococcus pneumoniae* (the pneumococcus) is a common commensal of this URT niche (1). However, translocation of the pneumococcus from the nasopharynx to the lungs, blood or the brain results in life-threatening disease (1). Indeed, among children under five years, *S. pneumoniae* is the leading cause of pneumonia deaths globally (2).

Using experimental human pneumococcal challenge (EHPC) of healthy volunteers and well-characterised epithelial cell models, we have previously shown that colonisation by *S. pneumoniae* is characterised by epithelial surface microcolony formation and invasion which we have called microinvasion (i.e. invasion of the epithelial barrier without disease) (3). The pneumococcal capsule is a major virulence determinant, influencing carriage, transmission from person to person, and invasive disease potential (4). Indeed, we have shown that *S. pneumoniae* epithelial microinvasion also varies markedly between strains expressing different capsular serotypes, with a serotype 4 strain invading Detroit 562 nasopharyngeal cell monolayers more readily than serotype 6B and 23F strains, and inducing more marked pro-inflammatory epithelial transcriptomic and cytokine responses (3).

We and others have previously proposed that although the epithelial innate immune response that results from pneumococcal colonisation may facilitate clearance, this highly variable pathobiont (>100 serotypes; >600 global pneumococcal sequence clusters (5)) tunes the host response to enhance transmission(3, 4). In addition to capsule, these processes have been shown to be

74 modulated by a broad array of subcapsular and cytoplasmic virulence factors (6), and more recently,
75 by bacterial carbohydrate, nucleotide, fatty acid and purine/ pyrimidine metabolism (7-11).

76

77 To explore the hypothesis that pneumococcal virulence has primarily evolved to promote
78 colonisation and subsequent transmission, but not necessarily disease, we have used a unique set
79 of *S. pneumoniae* serotype 6B Δ*proABC* and Δ*fhs* biosynthesis gene mutants developed to induce
80 protective immunity without causing disease (12). *proABC* and *fhs* were chosen as targets through
81 the analysis of previously published transcriptome and transposon mutational screens (11, 13, 14).
82 The *proABC* operon, consisting of genes predicted to encode a γ-glutamyl phosphate reductase
83 (*proA*), a γ-glutamyl kinase (*proB*) and a pyrroline-5-carboxylate reductase (*proC*), and *fhs* predicted
84 to encode a folate tetrahydrofolate reductase involved in one carbon metabolism pathways have
85 been implicated in metabolic adaptation to growth (15-17), and are highly transcribed in mouse
86 models of pneumococcal infection (16, 17). To further avoid reversion to a disease-causing
87 phenotype during EHPC, these mutants also contain a deletion of *piaA* which encodes the lipoprotein
88 component of the dominant pneumococcal iron uptake ABC transporter (18, 19). We have previously
89 shown that in a murine model, when compared to the *S. pneumoniae* serotype 6B wild-type parent
90 strain (WT, BHN418), the Δ*proABC/piaA* and Δ*fhs/piaA* mutants colonise the nasopharynx as
91 effectively. However, despite expressing the same capsule as the wild type 6B strain, neither the
92 Δ*proABC/piaA* and Δ*fhs/piaA* 6B strains causes invasive disease (12) (17). We have subsequently
93 shown that this attenuated phenotype is at least in part due to impaired growth in serum and is
94 associated with increased oxidative stress and altered lipid profiles (17). In EHPC, we have also
95 shown that both Δ*proABC/piaA* and Δ*fhs/piaA* retain the ability to colonise the human host, and can
96 induce IgG-mediated immunity (20). Therefore, these otherwise isogenic strains allow us to compare
97 the pneumococcal-epithelial interactions of disease-causing and non-disease-causing phenotypes,
98 while avoiding the confounding of differences in capsular serotype.

99

100 Here, we reveal that although the *S. pneumoniae* Δ*proABC/piaA* and Δ*fhs/piaA* metabolic function
101 mutations result in disease attenuation, the ability of the mutant strains to colonise and cause
102 microinvasion in both EHPC and *in vitro* epithelial infection models is preserved. Crucially, we also
103 show that despite similar patterns of epithelial cellular engagement, disruption of these key
104 pneumococcal metabolic pathways has differential effects on cellular reorganisation and innate
105 responses, which we propose influences niche adaptation during colonisation.

106

107 **RESULTS**

108

109 ***S. pneumoniae* 6B with Δ*proABC* or Δ*fhs* mutants colonise in EHPC with evidence of epithelial**
110 **microinvasion**

111 We have defined microinvasion as the process by which *S. pneumoniae* invades the mucosal
112 epithelium, inducing an innate immune response, without necessarily causing disease (Fig 1A).
113 Nasal curette samples from EHPC healthy volunteers inoculated with the *S. pneumoniae* serotype
114 6B WT or isogenic mutant strains *(*Δ*proABC/piaA* or Δ*fhs/piaA*) (21) were collected to investigate the
115 extent of epithelial association and microinvasion. A positive carrier was defined as colonisation at
116 any time point (day 2 or day 6 post-inoculation), as detected by microbiology culture (3). Visualisation
117 of the mucosal cells by confocal microscopy showed colonisation by the WT and mutant
118 pneumococcal strains (Fig 1B). At day 6 post challenge, compared to WT, there was no attenuation
119 of microinvasion with either the Δ*proABC/piaA* or Δ*fhs/piaA* strains, with a trend for greater
120 microinvasion (Fig 1C) with a higher microinvasive index (percentage of internalised bacteria /
121 associated bacteria; Supplemental Information Table 1).

122

123 **Fig 1. Pneumococcal – epithelial interactions in the EHPC model**. (A) Schematic showing that
124 during colonisation, pneumococci adhere to the epithelial cell surface (association), internalise inside
125 epithelial cells (microinvasion). Mucus – lime; pneumococci – purple; intracellular vacuole – dark
126 green; epithelial cells – yellow; nucleus – brown; cell junctions – pink. (B) Representative microscopy

127 images showing 6B association to the epithelium and microinvasion by the Δ*proABC/piaA* or
128 Δ*fhs/piaA* mutants. Surface carbohydrates (red), nuclei (DAPI, blue), pneumococci (green). (C)
129 Table summarising the percentage of bacteria that were found by microscopy, on the surface
130 (association) or inside (microinvasion) cells in the EHPC model. Mucosal curettage samples were
131 collected at day 6 post-pneumococcal challenge. Number of volunteers (n) in each group is indicated
132 in brackets, along with the total numbers of pneumococci (Spn) counted.

133

134

135 ***S. pneumoniae* colonisation and microinvasion of primary human airway epithelium leads to**
136 **cellular reorganisation with retention of barrier function**

137 To further explore the impact of microinvasion on epithelial biology in a complex environment, we
138 cultured *S. pneumoniae* serotype 6B WT and the isogenic biosynthesis mutants with primary normal
139 human bronchial epithelial airway (NHBE-A) cells in air-liquid interface. We observed epithelial cell
140 association and microinvasion with all three strains (Fig2A, top). TEM demonstrated that intracellular
141 bacteria for all three strains were enclosed within vacuoles (Fig 2A, bottom). As seen previously with
142 several different pneumococcal strains (3), the 6B WT and the mutant strains co-localised with
143 Junctional Adhesion Molecule A (JAM-A, Supplemental Information Fig 1A, arrow), with no change
144 in overall JAM-A expression. However, using confocal microscopy and automated image analysis,
145 for cells infected with the 6B WT strain, we did observe an increase in the intensity of Zonula
146 Occludens 1 (ZO-1) staining at the junctional membrane (Supplementary Fig 1B), and a significant
147 increase in the intensity of β catenin staining for cells infected with either the Δ*proABC/piaA or*
148 Δ*fhs/piaA* strain (Fig 2B, 2C). These changes in junctional protein expression most likely occurred
149 as a result of cellular reorganisation, as de-novo protein production would have been insufficient
150 over the 6-hour experimental infection period. As measured by transepithelial electrical resistance,
151 barrier integrity was retained over the infection period, (Fig 2D).

152

153 **Fig 2. Impact of pneumococcal infection on NHBE-A cell junctional protein expression and**
154 **barrier integrity.** NHBE-A Cells were cultured at ALI and infected with pneumococcal strains for

155 6hrs. (A) Top: Representative confocal microscopy images from 4 independent experiments with
156 replicates, showing pneumococcal (green) association with the epithelium (red, surface
157 carbohydrates; nuclei blue) at 6hr post infection. Bottom: Representative transmission electron
158 microscopy images from 2 independent experiments, showing pneumococcal microinvasion
159 examples of each strain (arrows), enclosed within a vacuole after 4hr infection. (B) Representative
160 confocal microscopy images from 4 independent experiments with replicates, showing
161 pneumococcal (green) interactions with junctional proteins (red) of β catenin. Colocalization of red
162 and green appears yellow. Nuclei (blue). (C) Integrated intensity of β catenin in pneumococcal
163 negative (not pneumococcal associated) or positive (pneumococcal associated) cells. Non infected
164 v pneumococcal negative cells **** p <0.0001 (NI v Δ*proABC/piaA*), ** p = 0.0026 (NI v Δ*fhs/piaA*);
165 non-infected v pneumococcal positive cells; **** p <0.0001 (NI v Δ*proABC/piaA* and NI v Δ*fhs/piaA*);
166 Kruskal-Wallis, n = 4 independent experiments. (D) Transepithelial electrical resistance (TEER) was
167 recorded pre- and post- 6hr infection to assess barrier integrity. N = 3 independent experiments with
168 replicates. Average TEER pre-infection was 466Ω.cm^2 (430-484 Ω.cm^2, p = 0.1458 ANOVA) and
169 average TEER post-infection was 545Ω.cm^2 (527-567 Ω.cm^2. p = 0.04744 ANOVA). Change in
170 TEER comparing non-infected cells to infected cells p = 0.6592, Kruskal-Wallis. Error bars represent
171 SEM.

172

173 When cultured at an air-liquid interface, NHBE cells differentiate into a typical pseudostratified
174 columnar ciliated epithelium, consisting of goblet, Clara, basal and ciliated cells (Fig 3A). Although
175 there was no predilection by *S. pneumoniae* for particular epithelial cell-types, pneumococci were
176 observed amongst cilia (acetylated tubulin positive cells, Fig 3B and Supplemental Information Fig
177 2) and co-localised with mucus (mucin5ac positive, Fig 3C, arrows). Strikingly, while the cellular
178 composition of the epithelial cultures exposed to the Δ*fhs/piaA* strain were comparable in
179 appearance to non-infected cells by SEM, exposure to the 6B WT and Δ*proABC/piaA* strains resulted
180 in an increased abundance in secreted mucus globules compared to non-infected cells (Fig 3A).
181 This appeared to be due to differential cellular secretion of preformed mucus rather than de-novo
182 production as these differences were not reflected in an increase in the expression of the gel-forming

183 glycoprotein Mucin5AC (Fig 3C and 3E, right graph). Following infection by the Δ*proABC/piaA* strain
184 we found a significant increase in expression of acetylated tubulin (Fig 3B and 3E, left graph), which
185 has been shown to be associated with increased microtubule conformation and elasticity, and occurs
186 by post-translational modification (22, 23). In contrast, following exposure to Δ*fhs/piaA* strain, we
187 saw an increased expression of the anti-inflammatory protein, uteroglobin (UG), which is a
188 multifunctional epithelial secreted protein with anti-inflammatory and anti-chemotactic properties,
189 and a marker for non-ciliated Clara cells (Fig 3D and 3F, left graph). These changes in UG
190 expression again most likely occurred as a result of cellular reorganisation, or secretion of pre-
191 formed protein, as de-novo protein production would have been insufficient to detect over the 6-hour
192 experimental infection period.

193

194

195 **Fig 3. Pneumococcal – epithelial interactions with primary human epithelial cells.** Cells were
196 cultured at ALI and infected with pneumococcal strains for 6hrs. (A) Representative scanning
197 electron microscopy images from 2 independent experiments, showing the surface of the epithelium.
198 Representative examples of differentiated epithelia (basal cells, Clara cells, goblet cells, ciliated
199 cells) are shown in yellow text. Colonising pneumococci are highlighted by arrows. Representative
200 confocal microscopy images from 4 independent experiments with replicates for (B) Ciliated cells
201 (acetylated tubulin, red), (C) Goblet cells (mucin5ac, red, (arrows indicate co-localisation of
202 mucin5ac with pneumococci)), (D) Clara cells (uteroglobin, red) after 6hr infection. Pneumococci
203 (green), nuclei (DAPI, blue), colocalization of red and green appears as yellow. (E) Integrated
204 intensity of acetylated tubulin and Muc5ac in pneumococcal negative or positive cells from two or
205 more images. Acetylated tubulin, neg p = 0.2677, pos p = 0.017; Mucin5ac, neg p = 0.6852, pos p =
206 0.8510, ANOVA. N = 3 or 4 independent experiments. (F) Integrated intensity of uteroglobin
207 normalised to non-infected cells (left, p = 0.0115 non-infected v infected, Kruskal-Wallis) and
208 percentage of Clara positive cells following infection (right, p = 0.0003 non-infected v strains, p =
209 0.0036 6B v mutant strains, Kruskal-Wallis). N = 3 independent experiments.

210

211 **Δ*proABC/piaA* and Δ*fhs/piaA* mutations of *S. pneumoniae* serotype 6B do not affect**
212 **microinvasion of Detroit 562 epithelial cells**

213 Detroit 562 epithelial nasopharyngeal cells enable the analysis of these host-pathogen interactions
214 under multiple conditions, which are not feasible with the primary cell lines. We have previously
215 shown that the pattern of Detroit 562 epithelial nasopharyngeal cell microinvasion, and subsequent
216 innate immune response to *S. pneumoniae* 6B infection *in vitro* is similar to that seen in the EPHC
217 *in vivo(3)*. We therefore then used Detroit 562 cells to further characterise colonisation by the WT,
218 Δ*proABC/piaA* and/or Δ*fhs/piaA* pneumococcal strains. We found that although all the strains formed
219 colonies on the epithelial surface (Fig 4A), the isogenic mutants associated less compared to 6B WT
220 (Fig 4B). Nonetheless, microinvasion was observed with all the strains (Fig 4C), with a significantly
221 elevated micro-invasive index for the Δ*proABC/piaA* and Δ*fhs/piaA* strains compared to WT (Fig 4D).
222 Differences in microinvasion were not due to differences in intracellular viability (Fig 4E) or replication
223 (Supplemental Information Fig 3A-F). All of the single and double biosynthesis genes mutants
224 (Δ*proABC*, Δ*fhs*, Δ*proABC/piaA*, Δ*fhs/piaA*) were impaired in their ability to transmigrate across the
225 epithelium (Fig 4F). Importantly, we show that a single Δp*iaA* mutation in the *S. pneumoniae* serotype
226 6B did not affect epithelial association, microinvasion and transmigration (Fig 4B, 4C, 4F).

227

228 **Fig 4**. **Strain association, microinvasion and transmigration of Detroit 562 cells.** Cells were
229 infected with *S. pneumoniae* for three hours and CFU counts recorded. (A) Representative confocal
230 microscopy images from 6 independent experiments with replicates, showing pneumococcal (green)
231 interactions with surface carbohydrates (red). (B) Association of pneumococcal strains to epithelial
232 cells. p = 0.0009 (Kruskal-Wallis), n = 6 with replicates. (C) Internalisation of strains into cells,
233 following a gentamicin protection assay. p = 0.0219 (Kruskal-Wallis) N = 6 with replicates. (D)
234 Microinvasive index is defined as the percentage of internalised bacteria over all associated bacteria.
235 p = 0.071 (Kruskal-Wallis) N = 6 with replicates. (E) Pneumococcal viability inside epithelial cells
236 following a gentamicin protection assay. n = 3 or 4 independent experiments with replicates. Counts
237 were normalised to microinvasion counts for each strain after 3 hours infection and compared to 6B

238 WT; +1hr p = 0.6517, +2hr p = 0.1377, +3hr p = 0.1183 (ANOVA). (F) Transmigration of
239 pneumococcal strains across confluent monolayers on transwell inserts. CFUs were recorded from
240 the basal chamber. N = 6 independent experiments with replicates. $p < 0.001$ (Kruskal-Wallis). (G)
241 Epithelial cell permeability was assessed via leak to 4kDa FITC-Dextran into the basal chamber. N
242 = 4 with replicates. $p < 0.0001$ compared to non-infected cells, and $p = 0.0689$ between 6B WT and
243 mutant strains (Kruskal-Wallis). (H) Representative confocal microscopy images from 6 independent
244 experiments with replicates, showing pneumococcal (green) interactions with β catenin (red).
245 Nuclear DAPI stain (blue). (I) Image quantification of integrated intensity of β catenin normalised to
246 non-infected cells, following infection with the different strains. N = 5 independent experiments. Non
247 infected v pneumococcal negative cells **** $p < 0.0001$ (NI v Δ*fhs/piaA*); non-infected v
248 pneumococcal positive cells; **** $p < 0.0001$ (NI v 6B), * $p = 0.0183$ (NI v Δ*proABC/piaA*), * $p = 0.0149$
249 (NI v Δ*fhs/piaA*); Kruskal-Wallis.

250

251 Consistent with our previous findings for serotype 6B(3), Detroit 562 epithelial barrier function was
252 not compromised after three hours of infection; indeed, there was a tightening of the barrier
253 evidenced by reduced FITC dextran diffusion after pneumococcal exposure (Fig 4G). Pneumococcal
254 infection had no effect on Junctional Adhesion Molecule A (JAM-A), Zonula-Occludens 1 (ZO-1),
255 Claudin 1 or Claudin 4 expression (Supplemental Fig 4). However, we did observe a significant
256 increase in epithelial β catenin expression following incubation with the Δ*proABC/piaA* and Δ*fhs/piaA*
257 strains, compared to the WT (Fig 4H, 4I).

258

259 **Δ*fhs/piaA* but not the ΔproABC/piaA mutations attenuate the pro-inflammatory epithelial**
260 **innate response to pneumococcal colonisation and microinvasion**

261 We have previously shown that the Detroit 562 cell innate immune response to *S. pneumoniae* is
262 strain dependent (3). Having found that serotype 6B biosynthesis gene mutants that are attenuated
263 for disease retain their capacity for microinvasion, we have further assessed the link between
264 colonisation, microinvasion and epithelial cell innate immunity by RNAseq. Compared to non-

265 infected cells (Fig 5A), all strains upregulated 78 core epithelial genes related to cytokine signalling
266 in immune system, NLR signalling and GPCR ligand binding. 193 genes were upregulated by both
267 the 6B WT and Δ*proABC/piaA* strains, characterised by Rhodopsin-like receptors, GPCR ligand
268 binding, cytokine signalling in Immune system, signalling by interleukins and Toll Receptor cascades.
269 Infection with the Δ*fhs/piaA* strain resulted in a markedly different transcriptomic profile with modest
270 upregulation of 254 genes, characterised by antigen processing, proteasomal pathways, GTP
271 hydrolysis, and intracellular stress responses (Fig 5A). Overall, the epithelial genes that were most
272 upregulated following infection with 6B WT or Δ*proABC/piaA* strain were similar and contrasted to
273 the reduced gene expression profile seen with the Δ*fhs/piaA* strain despite high levels of cell invasion
274 (Fig 5B). Since both mutant strains contained the *piaA* mutation, this could not account for the
275 differences seen in these responses. Together, these data demonstrate that microinvasion, the
276 innate epithelial response and disease are not necessarily linked.

277

278 **Fig 5. Detroit 562 cell transcriptomic responses to pneumococcal strains.** Epithelial cells were
279 infected for four hours with pneumococcal strains and RNA extracted and processed for RNAseq.
280 6B n = 11, PP n = 17, FP n = 14, non-infected n = 12, from 6 independent experiments. (A) All
281 significantly log2 fold change upregulated genes according to strain compared to non-infected cells.
282 Significance was defined as DEGs with a log2 fold change (logFC) of > 1.5 and false discovery rate
283 (FDR) of < 0.05. (B) Comparison of the top 20 most upregulated genes for each strain, compared to
284 non-infected cells. Upstream regulator analysis for (C) transcription factors and (D) kinases.

285

286 Transcription factors, cellular kinases and cytokines (Fig 5C, 5D) predicted to regulate the
287 differentially expressed genes, showed the greatest difference in profile following infection with
288 Δ*fhs/piaA* strain compared to infection with 6B WT and Δ*proABC/piaA* strains. Δ*fhs/piaA* was
289 predicted to show diminished NFκB and MAPK activation and was associated with a more intrinsic
290 and epithelial repair response that included TBK1, Raf1, JAK1 kinases and IL-1 and IL-33 cytokine
291 signalling.

292

293 **Enhanced epithelial caspase 8 activity following pneumococcal infection with the wild-type**
294 **and ∆proABC/piaA strains**

295 The NLRP3 inflammasome drives programmed epithelial cell death via caspase 1, caspase 3/7 and
296 caspase 8 activity (24). Caspase activity, primarily regulated post-translationally, enables a rapid
297 response to cellular stress and pathogen-mediated activation (25). In health, caspase regulation is
298 thought to be important for mucosal integrity (26). During bacterial pneumonia, caspase activation is
299 thought to have an important pro-inflammatory role, possibly triggered by pneumolysin (27, 28). We
300 have therefore explored whether the different patterns of microinvasion and epithelial reorganisation
301 seen with the WT 6B, and mutant strains are associated with differential caspase activation.

302

303 Compared to non-infected cells, infection with all strains led up to a 1.5-fold increase in epithelial
304 caspase activity 6-hour post infection (Fig 6A, dark grey bars). To test which caspases were
305 activated, we incubated infected cell cultures with either a caspase 1 inhibitor (YVAD-CHO), a
306 caspase 3/7 inhibitor (Z-VAD-FMK), or specifically measured caspase 8 activity. We found that the
307 increase was not due to caspase 1 activity (Fig 6B). Compared to non-infected cells, caspase 3/7
308 accounted for 3% and 15% of the caspase activity induced following infection with 6B WT and
309 ∆*fhs/piaA* strain respectively (Fig 6A). In contrast, ∆*proABC/piaA* strain did not induce caspase 3/7
310 activity. Significant caspase 8 activation was seen following infection with 6B WT and ∆*proABC/piaA*
311 strain, but not with the ∆*fhs/piaA* strain (Fig 6C).

312

313

314 **Fig 6. Effects of pneumococcal infection on caspase activity in Detroit 562 cells.** Caspase
315 activity was assessed by luminescence, following infection with pneumococcal strains for 6 hours.
316 (A) Caspase 3/7 activity was determined following incubation with the specific inhibitor Z-VAD-FMK.
317 N = 4 with replicates. In comparison to non-infected cells, caspase 3/7 $p = 0.0022$; caspase 3/7 + Z-

318 VAD-FMK inhibitor p = 0.0005. In comparison to 6B WT, caspase 3/7 p = 0.0215; caspase 3/7 + Z-
319 VAD-FMK inhibitor p = 0.0012 (Kruskal-Wallis). (B) Caspase 1 activity was determined following
320 incubation with the specific inhibitor YVAD-CHO. Negative signals indicate caspase activity other
321 than caspase 1. N = 6 with replicates. In comparison to non-infected cells, p = 0.39; caspase+YVAD-
322 CHO inhibitor p = 0.3604 and, in comparison to 6B WT, p = 0.6226; caspase+YVAD-CHO inhibitor
323 p = 0.5386 (Kruskal-Wallis). (C) Caspase 8 activity was assessed following infection with
324 pneumococcal strains. N = 3 with replicates. In comparison to non-infected cells, p = 0.0015
325 (ANOVA) and, in comparison to 6B WT, p = 0.0172 (ANOVA).

326

327 Together, these data suggest differential caspase induction following infection with the different
328 strains, linking the proinflammatory profile of the 6B WT and the Δ*proABC/piaA* with caspase 8
329 activation, which we postulate may regulate pneumococcal survival and transmission during
330 colonisation in the nasopharynx.

331

332 **Deletion of the *proABC* and *fhs* genes have broad-ranging differential effects on the *S.***
333 ***pneumoniae* virulence gene expression and metabolic gene pathways when under stress**

334 We have previously found marked transcriptional differences between the WT and both mutants in
335 response to serum stress (used to represent the physiological stress found during human infection),
336 with an over three-fold increase in the number of genes upregulated by the mutant strains compared
337 to WT (17). Further analysis revealed that these genes include well-characterised pneumococcal
338 virulence factors such as *ply*, *nanA*, *psaA,* those regulating oxidative stress such as *SpxB*, *lctO* and
339 *adhE*, and genes involved in purine and carbohydrate metabolism (Supplemental Information Table
340 2). Phosphotransferase systems, amino nucleotide sugar, fructose and mannose and metabolic
341 pathways were the most significantly enriched pathways in the Δ*proABC* mutant under serum stress
342 (Table 1). In contrast, competence, purine, pyruvate, metabolic pathways, amino nucleotide sugar
343 pathways and secondary metabolites were the most significantly enriched pathways in the Δ*fhs*
344 mutant under stress (Table 1). Together these data suggest that deletion of the *proABC* and *fhs*

345 genes have widespread but differential effects on *S. pneumoniae* virulence and metabolism which
346 may explain then complex phenotypes seen following epithelial infection.

347

348 **Table 1. Differentially expressed pathways from single isogenic mutants in human serum**
349 **compared to WT.**

Pathway	GeneRatio	P-adjust	qvalue
Δ*fhs* vs. WT			
Fatty acid metabolism/biosynthesis	10/57	1.08E-09	6.49E-10
Biosynthesis of secondary metabolites	26/57	2.09E-04	1.26E-04
Purine metabolism	10/57	1.34E-03	8.06E-04
Quorum sensing	11/57	3.20E-03	1.92E-03
Pantothenate and CoA biosynthesis	5/57	3.59E-03	2.16E-03
beta-Lactam resistance	5/57	7.59E-03	4.57E-03
Propanoate metabolism	4/57	1.51E-02	9.09E-03
2-Oxocarboxylic acid metabolism	4/57	1.51E-02	9.09E-03
Metabolic pathways	40/57	1.94E-02	1.16E-02
Amino sugar and nucleotide sugar metabolism	7/57	4.22E-02	2.54E-02
Pyruvate metabolism	5/57	4.31E-02	2.59E-02
Δ*proABC* vs. WT			
Fatty acid metabolism/biosynthesis	10/71	1.17E-08	8.94E-09
Galactose metabolism	12/71	1.25E-04	2.47E-08
Phosphotransferase system (PTS)	13/71	2.54E-03	1.93E-03
Amino sugar and nucleotide sugar metabolism	9/71	2.89E-02	2.20E-02

350

351

352 **Table 1. Differentially expressed pathways from single isogenic mutants in human**
353 **serum compared to WT.** 55 genes were selected within competence pathways, amino acid
354 metabolism, virulence factors, oxidative stress pathways and other known genes important
355 for colonisation, for assessment of changes in gene expression following serum stress. *q-*
356 *value* measures the proportion of false positives incurred (the false discovery rate) when
357 that particular test is significant.

358

359 ***fhs* gene mutation in *S. pneumoniae* 6B is associated with increased pneumococcal hydrogen**
360 **peroxide secretion and decreased pneumolysin activity**

361

362 *S. pneumoniae* SpxB and LctO generate hydrogen peroxide (H_2O_2) which has been shown to
363 suppress ENaC-α transcription and inhibit the Na+–K+ pump, acting as an intracellular signal to
364 increase mitochondrial production of ROS (29, 30). We therefore postulated that differential
365 expression of pneumococcal H_2O_2 may modulate epithelial functional responses during
366 nasopharyngeal colonisation by *S. pneumoniae* and explain the differences in the epithelial innate
367 immune response to the 6B WT, Δ*proABC/piaA* and Δ*fhs/piaA* strains. To assess this, we measured
368 H_2O_2 concentration using a luminescence-based bioassay, normalising against bacterial CFU. After
369 three and six hours, we detected significantly higher levels of H_2O_2 in Δ*fhs/piaA* cultures compared
370 to 6B WT and Δ*proABC/piaA* strains (Fig 7A). Furthermore, this was not ameliorated by epithelial
371 cell contact (Fig. 7B).

372

373 **Fig 7. Hydrogen peroxide secretion and pneumolysin activity from pneumococcal strains in**
374 **the absence and presence of Detroit 562 cells.** A) Fold change of hydrogen peroxide production
375 from the mutants compared to WT, normalised to the CFU counts. 3hr p = 0.0087 (ANOVA), 6hr p
376 = 0.0209 (Kruskal-Wallis). B) Fold change of hydrogen peroxide production from the mutants
377 compared to WT, normalised to the CFU counts, following infection of Detroit 562 cells. Media was

378 replaced after 1hr infection and cells incubated for a further 5hrs. N = 3 independent experiments
379 with replicates. Compared to 6B WT, p = 0.0034 (ANOVA). C) Pneumolysin activity was assessed
380 using a red blood cell lysis assay. Strains were incubated with red blood cells for 30 minutes and
381 absorbance measured. N = 4 experiments with replicates. Pneumococcal strain haemolytic activity
382 is calculated in comparison to 100% lysis by 0.0625% saponin. p <0.0001 compared to 6B WT
383 (ANOVA).

384

385 The pore forming pneumococcal toxin pneumolysin can both activate and suppress the host innate
386 immune response and mediates the haemolytic activity characteristic of the pneumococcus (31-33).
387 H_2O_2 can increase the release of pneumolysin but paradoxically also negatively impairs its
388 haemolytic activity (34). Compatible with the latter and the higher production of H_2O_2 by the Δ*fhs*
389 */piaA* strain, despite having increased expression of *ply*, red blood cell lysis was reduced for Δ*fhs*
390 strains compared to 6B WT and Δ*proABC* (Fig. 7C).

391

392 Differential pneumococcal H_2O_2 release may therefore explain at least in part, the effects of the *S.*
393 *pneumoniae* serotype 6B WT and Δ*proABC /piaA* compared to the Δ*fhs /piaA* strain on the epithelial
394 response to colonisation and microinvasion. Importantly, in the 6-hour timeframe assessed, the
395 increased H_2O_2 release the Δ*fhs /piaA* strain was not associated with epithelial cellular toxicity or
396 loss of barrier function, but was associated with increased intracellular epithelial stress response, as
397 detected by RNAseq.

398

399 **DISCUSSION**

400 There is considerable variation in the propensity of different *S. pneumoniae* strains to colonise the
401 human host, cause invasive disease and transmit to others (1). During colonisation of the
402 nasopharyngeal niche, the pneumococcus was previously thought to be confined to the mucus layer
403 and the epithelial surface (1). However, using EHPC, we have previously reported that

404 pneumococcal microinvasion occurs in healthy volunteers (3), and we now show that even when
405 using isogenic serotype 6B pneumococcal biosynthesis pathway mutant strains that are attenuated
406 for systemic disease but not for carriage, this microinvasion is preserved (12). We found that
407 pneumococcal colonisation and microinvasion of primary human airway epithelium led to cellular
408 reorganisation and mucus production while retaining barrier function, although the pattern of this
409 reorganisation varied by strain. Furthermore, the pro-inflammatory innate response and caspase 8
410 activity associated with epithelial infection by *S. pneumoniae* serotype 6B were attenuated by the
411 Δ*fhs/piaA* but not by the Δ*proABC/piaA* mutation. Under stress conditions, along with presumably
412 compensatory changes in the expression of multiple metabolic pathways, the Δ*proABC* and Δ*fhs*
413 mutations resulted in the upregulation of several pneumococcal virulence factor genes (Graphical
414 Abstract Summary). Notably, the *fhs* gene mutation in *S. pneumoniae* serotype 6B was associated
415 with increased pneumococcal hydrogen peroxide secretion and decreased pneumolysin activity.
416 Together these findings suggest that despite being attenuated for disease, the metabolic changes
417 and the increased expression of pneumococcal virulence genes in response to stress may explain
418 the preservation of epithelial microinvasion by these mutants. However, although epithelial
419 microinvasion, cellular reorganisation, innate immune response, and the propensity to cause
420 invasive disease are strain dependent, these properties do not appear to be directly co-correlated.

421

422 **Graphical Abstract**

423 *S. pneumoniae* colonisation is characterised by mucus association, epithelial adherence and
424 microinvasion – where the pneumococcus invades the epithelial barrier without causing disease.
425 Microcolonies form at the epithelial surface and pneumococcal transmigration can occur between
426 epithelial cells. Although mutations in *S. pneumoniae* biosynthesis genes (Δ*proABC* and Δ*fhs*)
427 attenuate disease in a murine model, they do not attenuate microinvasion in either experimental
428 human pneumococcal challenge (EHPC) or *in vitro* in primary and immortalised epithelial cells.
429 These mutations show strain-dependent effects on both the epithelial and bacterial responses to
430 infection. While not directly co-correlated, factors such as epithelial cellular reorganisation,
431 inflammation and caspase 8 activity alongside pneumococcal metabolic adaptation, virulence factor

432 expression and response to stress are key determinants of the outcome of colonisation in the
433 nasopharyngeal niche.

434

435

436 The complexity of the interaction between *S. pneumoniae* and the mucosal epithelium was
437 highlighted through infection of our well-characterised primary epithelial cell model(35). The model
438 consisting of Clara cells (involved in secretory, xenobiotic metabolic, and progenitor cell functions),
439 goblet cells (mucus production), ciliated cells (responsible for mucus and small particle transport),
440 exhibited considerable epithelial cellular re-organisation involving β catenin, acetylated tubulin and
441 uteroglobin in response to pneumococcal infection. In a rabbit pneumococcal meningitis model,
442 increased acetylated tubulin and microtubule stabilisation was attributed to pneumolysin activity(23).
443 Previously, using a pneumolysin deficient mutant of *S. pneumoniae* serotype 4 (TIGR4), we have
444 shown that pneumolysin is a key driver of the epithelial inflammatory response to pneumococcal
445 infection (3). We therefore speculate that the differential expression of pneumolysin and H_2O_2 by the
446 WT and mutant strains may contribute to the differing patterns of epithelial reorganisation, and goblet
447 cell mucus release that we observed, and may impact on both clearance and transmission (1).

448

449 Epithelial infection with the 6B WT and Δ*proABC/piaA* strains induced innate inflammatory pathway
450 gene expression typical of pneumococcal infection (3), including cytokine/chemokines, interleukins,
451 Toll Like Receptor and NFκB signalling, alongside apoptotic transcripts such as FOXO3 and TP53.
452 We also identified epithelial genes upregulated only during WT infection, potentially related to a
453 greater disease-causing potential. These genes are involved in RNA degradation, O-linked
454 glycosylation, wnt signalling, DNA sensing, RIG-I pathways and signal transduction. In contrast, the
455 Δ*fhs/piaA* strain activated a pro-survival and adaptation profile, upregulating genes such as JUN,
456 SMARCA4, NFAT5, KLF6 and TCF4, which are involved in homeostatic signalling and chromatin
457 remodelling (36, 37), suggestive of a more tolerant response. Ultimately, these capsule-independent
458 differences in pneumococcal-epithelial interactions may shape the adaptive immune response to

459 pneumococcal colonisation (21, 38), which could then further influence the outcomes of both
460 colonisation and disease. How these findings translate to differences in the duration of
461 nasopharyngeal carriage, invasiveness, transmission or clearance remains to be fully determined.
462 However, during EHPC, Δ*fhs/piaA* infection was associated with increased density at day 6 post-
463 inoculation compared the other strains (20).

464

465 Importantly, while WT serotype 6B infection led to epithelial cell reorganisation (β catenin localisation
466 to the junctional membrane and mucus secretion), pneumococcal transmigration, a more pro-
467 inflammatory innate immune transcriptomic profile and increased caspase 8 activity, all indicative of
468 a robust cellular response to *S. pneumoniae*, the Δ*fhs/piaA* but not Δ*proABC/piaA* strains was
469 attenuated for many of these characteristics. This suggests that similar to the macrophage response
470 to *S. pneumoniae*, intracellular signalling by pneumococci is not the sole determinant of the epithelial
471 response to infection (32, 39). The *proABC* operon consists of three genes involved in proline
472 biosynthesis (ProABC)(40). *fhs* catalyses the synthesis of N10 formyl tetrahydrofolate, essential for
473 carbon metabolism and purine nucleotide biosynthesis in various bacterial species (16, 41),
474 especially under hypoxic conditions (41, 42). It is increasingly recognised that bacterial virulence and
475 metabolism are intimately linked (43). Whether the distinct epithelial innate immune response to
476 Δ*fhs/piaA* infection is due to diminished epithelial NFκB and MAPK activation (potentially linked to
477 extracellular receptor engagement), reduced caspase 8 activity mediated by enhanced
478 pneumococcal H_2O_2 release, decreased pneumolysin activity, or a compensatory metabolic
479 response to the stress remains to be determined.

480

481 *S. pneumoniae* is highly adapted to colonise the human host and transmit from person to person.
482 Invasive pneumococcal disease, particularly in its most severe forms, is a dead end for the bacteria.
483 Our observation that the induction of inflammation/ innate immunity is not necessarily linked to
484 disease potential supports our proposition that microinvasion during colonisation by the
485 pneumococcus may facilitate immune evasion. As is typical of 'professional' intracellular bacterial

486 species such as *Listeria* and *Salmonella*, the resulting host response might also promote
487 transmission (44, 45). Whether the less pro-inflammatory Δ*fhs/piaA* is less transmissible than the
488 more inflammatory WT remains to be determined but this could be further explored using EHPC
489 (46).

490

491 In conclusion, these data further support our proposed paradigm that epithelial microinvasion by *S.*
492 *pneumoniae* in healthy people is frequent and usually does not lead to disease. Our findings highlight
493 the broad-ranging effects of even single gene mutations in pneumococcal biosynthesis pathways,
494 which may partially explain the complexity of differences between seemingly closely related strains.
495 However, strain differences in subsequent epithelial cell microinvasion, cellular reorganisation and
496 inflammatory responses are likely driven by differential expression of a range of bacterial virulence
497 and metabolic pathways that are not necessarily co-correlated with disease-causing potential. As
498 suggested by our bacterial transcriptomic data, no single pneumococcal virulence factor or group of
499 factors fully explains the differences seen between the strains under stress. The complexity of these
500 bacterial-host cell interactions is modulated by mediators such as hydrogen peroxide and
501 pneumolysin, which can have both enhancing and inhibitory effects on the epithelial cell response to
502 infection in different contexts. *S. pneumoniae* in constantly evolving, with new variants emerging
503 both due to stochastic events and under ecological pressure from numerous factors including
504 vaccines and antibiotic exposure (47, 48) (49). Extensive phenotyping of emerging, genotypically
505 related pneumococcal strains offers the opportunity to more effectively unravel *S. pneumoniae*
506 pathogenesis and its adaptation to the nasopharyngeal niche.

507

508 **METHODS**

509

510 **Bacteria**

511 The *Streptococcus pneumoniae* serotype 6B (strain BHN 418(50)) was a kind gift from Prof. Birgitta
512 Henriques Normark (Karolinska Institute). Δ*proABC/piaA* and Δ*fhs/piaA* mutant strains were

513 generated using overlap extension PCR as described by Ramos-Sevillano *et al*(12). Stocks of
514 bacteria were stored at -80°C when bacterial growth in Todd Hewitt Broth (THY) was 0.3 $O.D._{600nm}$.
515 Aliquots were defrosted, centrifuged at 8000g for eight minutes and resuspended in 1% Fetal Bovine
516 Serum (FBS, Gibco) in MEM media (Gibco) for infections. Approximately 10 bacteria were added for
517 every epithelial cell. Colony forming units (CFU) were counted by serial dilutions on horse blood agar
518 plates (EO Labs). Starting inoculums were not significantly different across strains for all assays.

519

520 **Bacterial RNA-seq sample collection, sequencing and reads**

521 Mutant pneumococcal strains (three biological replicates for each mutant) and 6B WT (three
522 biological replicates) were grown in THY to mid log phase and the pellets resuspended in THY and
523 undiluted human serum for 60mins. The culture was then pelleted, and RNA stored in RNA Protect
524 at -70°C before extracting total RNA (17). Total RNA from each library was ribo-depleted and sent
525 for Illumina Next Seq Sequencing Pathogen Genomics Unit (PGU), UCL. The quality of raw FASTQ
526 reads was checked by FastQC v0.11.5, Babraham Bioinformatics, UK (51) and visualised using
527 multiQC v1.9 (52). Reads were trimmed using Trimmomatic 0.39 (53). Trimmed reads were also
528 checked by FastQC and multiQC. Trimmed reads were then mapped to KEGG annotated 6B
529 genome sequence (670-6B, Accession: CP002176.1) using bowtie2 with default settings(54).
530 Conversion into BAM files was performed using SAMtools (55). Mapped reads were visualized in
531 the Integrated Genome Browser (IGB) (56). FeatureCounts v2.0.0 was used to summarize read
532 counts for each annotated feature in the respective reference genomes in multimapping mode (-M)
533 (57).

534

535 **Differential gene expression analyses**

536 The generated count matrix was imported into R-studio (R v3.4.2) and normalization of counts and
537 differential gene expression analysis was performed by DESeq2 (58). DESeq2 normalized libraries
538 were regularized log transformed for visualizing heatmaps and clustering. Differential gene
539 expression was performed on raw counts. Fold change shrinkage was implemented with the apeglm

540 package within DESeq2. Genes with a log2 fold change > 1.5 and false discovery rate (FDR) of <
541 0.05 were categorized as differentially expressed. KEGG pathway enrichment and module analysis
542 were performed on differentially regulated genes using over representation analysis (ORA)
543 implemented by clusterProfiler (59).

544

545 **Experimental Human Pneumococcal Carriage Model (EHPC)**

546 A full explanation of experimental design and selection criteria has been previously described (3).
547 Following written informed consent, healthy non-smoking adults between the ages of 18 – 59 were
548 inoculated with 80,000 CFU/nostril live strains of *S. pneumoniae*. Mucosal cells from the inferior
549 turbinate using a plastic Rhino-probe™ (curettage, Arlington Scientific) were collected prior to
550 inoculation, and days 2 and 6 post-inoculation. Samples were processed for confocal microscopy
551 analysis. Nasal wash samples were collected for CFU count analysis. There were no adverse events.
552 Ethical approval was given by NHS Research and Ethics Committee (REC)/Liverpool School of
553 Tropical Medicine (LSTM) REC, reference number: 18/NW/0481 and Human Tissue Authority
554 licensing number 12548.

555

556 **Primary Human Epithelial Cells**

557 Normal Human Primary Bronchial/Tracheal Epithelial Cells (NHBE-A, ATCC® PCS-300-010™) were
558 plated at $6x10^3$ cells/cm^2 on a layer of sub-lethally γ-irradiated (60 Gy) mouse embryonic fibroblasts
559 3T3-J2 cells (kind donation from Howard Green, Harvard Medical School, Boston(60)) with
560 keratinocyte culture medium cFAD (3:1 DMEM (Gibco) to Ham F-12 Nut Mix (Gibco), 10% FBS
561 (HyClone, Sigma), 1% Penicillin-Streptomycin (100X, Sigma), 0.4 µg/mL Hydrocortisone
562 (Calbiochem, USA), 5 µg/ml Insulin (various), 10-10 Cholera Toxin (Sigma) and 2x10-9
563 Triodothyronine (Sigma)). Epithelial cells were stimulated with 10 ng/mL human epidermal growth
564 factor (hEGF, PeproTech, USA) on days 3 and 5. Cultures were grown at 37°C 6% CO_2 and sub-
565 confluent cultures were trypsinised with 0.25% Trypsin-EDTA (Sigma). For NHBE-A differentiation
566 in Air Liquid Interface (ALI) culture, cells were plated at a density of $6x10^4$/cm^2 on 1µm pore PET cell

567 culture inserts (12 wells, Greiner). The insert was supplemented with cFAD medium on the top and
568 bottom. After 48 hours, medium was removed from the top of the culture (exposure) and the culture
569 was fed with fresh PneumaCult™ differentiation Medium (Stemcell Technologies) from the bottom
570 of the well every 2 days for 3 weeks, until cell ciliation was observed. Antibiotics were removed from
571 the medium and cells washed 24 hours before infection experiments.

572

573 **Human Epithelial Cell Lines**

574 Human pharyngeal carcinoma Detroit 562 epithelial cells (ATCC_CCL-138) were grown in 10% FCS
575 in alpha MEM media (Gibco). For each set of experiments, cells were used within 5 passages. Cells
576 consistently tested PCR negative for mycoplasma (Cambridge Biosciences).

577

578 **Pneumococcal-epithelial cell co-culture**

579 For association and internalisation assays, confluent monolayers of Detroit 562 cells (typically day 7
580 - 8 post plating) cultured on 12 well plates (Corning), were exposed to *S. pneumoniae* (1 cell : 10
581 pneumococci) for three hours in 1% FCS alpha MEM (six-hour infection for HNBE-A cells in 1%
582 Pneumocult media without supplements) (3). Cells washed three times in $HBSS^{+/+}$ before incubation
583 in 1% saponin for 10 minutes at 37ºC to lyse cells. Bacterial dilutions were plated on horse blood
584 agar for 16 hours and colony forming units counted. For internalisation quantification, 200µg/ml
585 gentamicin was added to the cells for one hour before incubation with saponin.

586

587 For transmigration assays, Detroit 562 cells were plated onto 3µm pore, PET Transwell Inserts
588 (ThermoFisher) typically for 10 days (3). Media was changed to 1% FCS (250µl apical chamber, 1ml
589 basal chamber) one hour prior to infection experiments. 1mg/ml FITC-dextran (Sigma Aldrich) was
590 added to the apical chamber of selected inserts for permeability assays. Transepithelial Electrical
591 Resistance (TEER) was measured before and after infection using an EVOM2 (World Precision
592 Instruments). Bacteria were added to the cells for three hours during of which 50µl of basal media
593 was repeatedly removed to measure bacterial load by counting CFU/well. Permeability was recorded
594 using a FLUOstar Omega (BMG Labtech) at 488nm.

595

596 **Confocal Microscopy**

597 Sample processing was performed as previously described(3). Briefly, mucosal cells from the EHPC
598 model were placed directly into 4% PFA and cytospun onto microscope slides. NHBE-A cells and
599 Detroit 562 cells cultured on transwell membranes were fixed in 4% PFA (Pierce, Methanol Free).
600 Cells were permeabilised with 0.2% Triton X-100 for 10 minutes, blocked for one hour in blocking
601 buffer (3% goat serum and 3% BSA in PBS (Sigma)) and incubated with pneumococcal antisera
602 Pool Q (raised against the polysaccharide capsule, SSI Diagnostica) for one hour. Wheat germ
603 agglutinin conjugated to Rhodamine (Vector Labs) was added along with goat-anti rabbit IgG
604 conjugated to Alexa Fluor 488 for 45 minutes in blocking buffer. Primary (used at 1:100) antibodies
605 used for epithelial cell proteins can be found in Supplemental Information Table 3. Secondary (used
606 at 1:500) antibodies were either goat anti-mouse or goat anti-rabbit – Alexa Fluor 555 or 546,
607 ThermoFisher. Of note, for epithelial protein antibodies raised in rabbit (Uteroglobin), no
608 pneumococcal staining was possible and therefore pneumococci were not visible on the images.
609 DAPI was added for 5 minutes and cells were mounted with Aqua PolyMount (VWR International)
610 and a coverslip on the microslide. Pneumococci were recorded by manual scanning of the whole
611 cytospin for the EHPC samples. More than three fields of view were recorded for each bacterial
612 strain for Detroit 562 cell infections, using inverted Zeiss LSM (either 700 or 880) confocal
613 microscopes. Images were processed with Zeiss LSM Image Browser. Z stacks were recorded at
614 1µm intervals at either 40x oil or 63x oil objectives. Automated image analysis was carried out using
615 Cellprofiler (61).

616

617 **Electron Microscopy**

618 Preparation of Detroit 562 cells and NHBE-A cells was identical, and previously described(3). Briefly,
619 cells cultured on transwells were fixed with 2% paraformaldehyde and 1.5% glutaraldehyde in 0.1 M
620 cacodylate buffer and post-fixed in 1% OsO4 / 1.5% K4Fe(CN)6 in 0.1 M cacodylate buffer pH7.3.
621 Samples were dehydrated in graded ethanol-water series and infiltrated with Agar 100 resin mix.
622 Ultra-thin sections were cut at 70-80 nm using a diamond knife on a Reichert ultracut microtome.

623 Sections were collected on 300 mesh copper grids and stained with lead citrate. For transmission
624 electron microscopy the samples were hardened at 60°C for 48 hours. The coverslip was removed,
625 and a representative area was selected. Ultra-thin sections were cut at 70-80 nm using a diamond
626 knife on a Reichert ultra-cut S microtome. Sections were collected on copper grids and stained with
627 lead citrate. Samples were viewed with a Joel 1010 transition electron microscope and the images
628 recorded using a Gatan Orius CCD camera.
629
630 **Pneumolysin activity**
631 Adapted from Kirkham et al(62). Briefly, final concentration of 2% horse blood (EO Labs) solution
632 was prepared in phenol free alpha MEM (Life Technologies) and 100 µl added to wells of a 96 U-
633 bottom plate (Corning). 100 µl of bacterial solutions (containing ~$2.5x10^6$ bacteria) were suspended
634 in phenol free alpha MEM were added to each 96 well. Saponin was used as a positive control for
635 lysis. Solutions were incubated for 30 minutes at 37°C before centrifugation at 1000g for one minute.
636 100 µl was transferred into a new 96 well plate and absorbance recorded at 540nm on a plate reader.
637
638 **Hydrogen Peroxide Assay**
639 Detroit 562 cells were cultured in white 96 well plates (Corning). NHBE-A cells were cultured in 12
640 well plates in Pneumocult media. Cells were incubated with H_2O_2 substrate and infected with strains
641 of *S. pneumoniae* for up to six hours according to manufacturers' instructions (ROS-Glo™ H_2O_2
642 Assay, Promega). ROS-Glo™ Detection solution was added to the cells and incubated for 20
643 minutes. For primary cells, supernatant was then transferred to a white 96 well plate. Luminescence
644 was read using a GloMax -Multi Detection System plate reader (Promega).
645
646 **Caspase assay**
647 Detroit 562 cells were cultured in white 96 well plates (Corning). NHBE-A cells were cultured in 12
648 well plates in Pneumocult media. Cells were infected with strains of *S. pneumoniae* for up to six
649 hours. Primary cell supernatant was transferred to a white 96 well plate. Samples were incubated
650 with Caspase-Glo® 1 Reagent, Caspase-Glo® 1 YVAD-CHO Reagent, Caspase-Glo® Z-VAD-FMK

651 Reagent or Caspase-Glo® 8 Reagent, for one hour and according to manufacturers' instructions
652 (Promega). Luminescence was read using a GloMax-Multi Detection System plate reader
653 (Promega).

654

655 RNA samples and sequencing (RNA-Seq)

656 RNA-Seq data was collected as previously described (3). Confluent monolayers of Detroit 562
657 epithelial cells were infected with S. pneumoniae strains for four hours before collection in RNALater.
658 RNA was extracted using a Qiagen RNAEasy micro kit and treated for DNA removal using a Qiagen
659 Turbo DNA-free kit. RNA quality was assessed and quantified using a BioAnalyser (Agilent 2100).
660 Samples were sequenced using Illumina Nextseq 500/550 High Output 75 cycle kit giving 15-20
661 million 41bp paired-end reads per sample (Pathogens Genomic Unit, UCL).

662

663 **Statistics**

664 Each condition within each experiment was performed in duplicate or triplicate, and each experiment
665 was performed independently more than three times, unless stated otherwise. Error bars represent
666 SEM, unless stated otherwise. GraphPad Prism Version 7 was used for parametric (t-tests or
667 ANOVA) or non-parametric (Mann-Whitney or Kruskal-Wallis tests) analysis, which was based on
668 the Shapiro-Wilk normality test. Ad hoc tests were performed using Tukey's (for parametric data) or
669 Dunn's (for non-parametric data) multiple comparisons test. P values less than 0.05 were considered
670 significant.

671

672 **Data and code availability**

673 Source data are provided as a Source Data file. RNAseq data from the Detroit 562 cell infections is
674 publicly accessible through Zenodo with Accession (DOI:10.5281/zenodo.7997789).

675

676 **ACKNOWLEDGEMENTS**

677 This study was funded by CMW from a Postdoctoral Innovation Award from UCL, a Pump-Priming
678 Award and Enhancement Award from the Human Infection Challenge Network for Vaccine
679 Development (HIC-VAC (funded by the GCRF Networks in Vaccines Research and Development)
680 which is co-funded by the MRC and BBSRC). This UK funded award is part of the EDCTP2
681 programme supported by the European Union. CMW and RSH are supported by the Medical
682 Research Council (grant MR/T016329/1). The authors would like to thank Prof. Peter Hermans
683 (Radboud University Medical Centre) for donating the 6B pneumococcal strain originally from Prof.
684 Birgitta Henriques-Normark (Karolinska Institute) and obtained directly from DF at LSTM. EHPC
685 sample collection was supported by the Medical Research Council (grant MR/M011569/1), Bill and
686 Melinda Gates Foundation (grant OPP1117728) awarded to DF and the National Institute for Health
687 Research (NIHR) Local Comprehensive Research Network. The authors also wish to thank the
688 EHPC Clinical Team at LSTM and all the volunteers. Confocal imaging facilities at LSTM were
689 funded by a Wellcome Trust Multi-User Equipment Grant (104936/Z/14/Z). Electron microscopy
690 processing and image capture was performed by Dr. Elizabeth Slavik-Smith in the Biosciences EM
691 facility at UCL. MC is supported by a Springboard to Independence grant (AirwayStasis) from the
692 French Government's Investissement d'Avenir program, the Laboratoire d'Excellence ''Integrative
693 Biology of Emerging Infectious Diseases" (ANR-10-LABX-62-IBEID) and the Chromatin and infection
694 unit headed by Melanie A. Hamon. RNA-Seq library preparation was undertaken at UCL through the
695 UCL/UCLH Biomedical Research Centre and MRC funded Pathogen Genomics Unit (PGU,
696 G0900950). All RNAseq data processing was completed by the PGU. MN is supported by the
697 Wellcome Trust and by NIHR Biomedical Research Centre Funding to University College Hospitals
698 NHS Foundation Trust and University College London. RR is supported by Marie Skłodowska-Curie
699 Individual Fellowships 896014. PB is supported by the European Research Council (ERC-Stg No.
700 639429), the Rosetrees Trust (M362-F1; M553), the CF Trust (SRC006;SRC020), the London
701 Advanced Therapies - Research England (C2N-AT.006), the MRC Confidence in Concept scheme
702 (Award: MC_PC_17180), the Innovate UK (Smart grant n.10005465), the Duchenne Parent Project
703 (DPP) and the NIHR GOSH BRC. MW is supported by a 223065 Wellcome Investigator Award to
704 Clare Jolly, UCL. ERS and JSB are supported by MRC grant R/N02687X/1 and Wellcome grant
705 221803/Z/20/Z. JSB is partially supported by the Department of Health's National Institute of Health

706 and Care Research Biomedical Research Centre funding to UCLH. RSH is a NIHR Senior
707 Investigator.

708

709 **AUTHOR CONTRIBUTIONS**: CMW conceived, funded, designed and conducted the study,
710 performed the experiments, acquired samples and processed data, and wrote the first draft of the
711 manuscript. GP analysed and interpreted the RNAseq data. MB analysed and interpreted the
712 bacterial transcriptomic data. RR cultured and differentiated primary epithelial cells. MC provided
713 manuscript writing support. ERS generated the 6B mutant strains and bacterial transcriptomic data.
714 JR collected and processed EHPC samples. JAGA processed the RNA-Seq data. MW ran the image
715 analysis. PB provided investigator support. MN provided RNA-Seq analysis support. DF provided
716 investigator support and EHPC clinical samples. JSB generated the 6B mutant strains, interpreted
717 the data and revised the manuscript. RSH provided investigator support, designed and interpreted
718 the data, revised the manuscript. All authors commented on and approved the manuscript.

719

720 **COMPETING INTERESTS:** The authors declare no competing interests.

721

722 **REFERENCES**

723 1. Weiser JN, Ferreira DM, Paton JC. Streptococcus pneumoniae: transmission, colonization and
724 invasion. Nat Rev Microbiol. 2018;16(6):355-67.
725 2. O'Brien KL, Wolfson LJ, Watt JP, Henkle E, Deloria-Knoll M, McCall N, et al. Burden of disease caused
726 by Streptococcus pneumoniae in children younger than 5 years: global estimates. Lancet.
727 2009;374(9693):893-902.
728 3. Weight CM, Venturini C, Pojar S, Jochems SP, Reine J, Nikolaou E, et al. Microinvasion by
729 Streptococcus pneumoniae induces epithelial innate immunity during colonisation at the human mucosal
730 surface. Nat Commun. 2019;10(1):3060.
731 4. Zafar MA, Hamaguchi S, Zangari T, Cammer M, Weiser JN. Capsule Type and Amount Affect Shedding
732 and Transmission of Streptococcus pneumoniae. mBio. 2017;8(4).
733 5. Gladstone RA, Lo SW, Lees JA, Croucher NJ, van Tonder AJ, Corander J, et al. International genomic
734 definition of pneumococcal lineages, to contextualise disease, antibiotic resistance and vaccine impact.
735 EBioMedicine. 2019;43:338-46.
736 6. Amin-Chowdhury Z, Collins S, Sheppard C, Litt D, Fry NK, Andrews N, et al. Characteristics of Invasive
737 Pneumococcal Disease Caused by Emerging Serotypes After the Introduction of the 13-Valent Pneumococcal
738 Conjugate Vaccine in England: A Prospective Observational Cohort Study, 2014-2018. Clin Infect Dis.
739 2020;71(8):e235-e43.

740 7. Echlin H, Frank M, Rock C, Rosch JW. Role of the pyruvate metabolic network on carbohydrate
741 metabolism and virulence in Streptococcus pneumoniae. Mol Microbiol. 2020;114(4):536-52.
742 8. Hartel T, Eylert E, Schulz C, Petruschka L, Gierok P, Grubmuller S, et al. Characterization of central
743 carbon metabolism of Streptococcus pneumoniae by isotopologue profiling. J Biol Chem. 2012;287(6):4260-
744 74.
745 9. Henriques-Normark B, Tuomanen EI. The pneumococcus: epidemiology, microbiology, and
746 pathogenesis. Cold Spring Harb Perspect Med. 2013;3(7).
747 10. Kohler S, Voss F, Gomez Mejia A, Brown JS, Hammerschmidt S. Pneumococcal lipoproteins involved
748 in bacterial fitness, virulence, and immune evasion. FEBS Lett. 2016;590(21):3820-39.
749 11. van Opijnen T, Camilli A. A fine scale phenotype-genotype virulence map of a bacterial pathogen.
750 Genome Res. 2012;22(12):2541-51.
751 12. Ramos-Sevillano E, Ercoli G, Felgner P, Ramiro de Assis R, Nakajima R, Goldblatt D, et al. Preclinical
752 Development of Virulence Attenuated Streptococcus pneumoniae Strains Able to Enhance Protective
753 Immunity Against Pneumococcal Infection. Am J Respir Crit Care Med. 2020.
754 13. Ogunniyi AD, Mahdi LK, Trappetti C, Verhoeven N, Mermans D, Van der Hoek MB, et al. Identification
755 of genes that contribute to the pathogenesis of invasive pneumococcal disease by in vivo transcriptomic
756 analysis. Infect Immun. 2012;80(9):3268-78.
757 14. Mahdi LK, Wang H, Van der Hoek MB, Paton JC, Ogunniyi AD. Identification of a novel pneumococcal
758 vaccine antigen preferentially expressed during meningitis in mice. J Clin Invest. 2012;122(6):2208-20.
759 15. Brill J, Hoffmann T, Bleisteiner M, Bremer E. Osmotically controlled synthesis of the compatible solute
760 proline is critical for cellular defense of Bacillus subtilis against high osmolarity. J Bacteriol.
761 2011;193(19):5335-46.
762 16. Crowley PJ, Gutierrez JA, Hillman JD, Bleiweis AS. Genetic and physiologic analysis of a formyl-
763 tetrahydrofolate synthetase mutant of Streptococcus mutans. J Bacteriol. 1997;179(5):1563-72.
764 17. Ramos-Sevillano E. EG, Guerra-Assunção J.F., Betts M., Partridge F., Fernandes V.E., Wall E., Gordon
765 S.B., Ferreira D.M., Heyderman R.S., Brown J.S. Essential role of proline synthesis and the one-carbon
766 metabolism pathways for systemic virulence of Streptococcus pneumoniae. Biorxiv. 2023.
767 18. Brown JS, Gilliland SM, Holden DW. A Streptococcus pneumoniae pathogenicity island encoding an
768 ABC transporter involved in iron uptake and virulence. Mol Microbiol. 2001;40(3):572-85.
769 19. Hill H, Mitsi E, Nikolaou E, Blizard A, Pojar S, Howard A, et al. A Randomised Controlled Trial of Nasal
770 Immunisation with Live Virulence Attenuated Streptococcus pneumoniae Strains Using Human Infection
771 Challenge. Am J Respir Crit Care Med. 2023.
772 20. Hill H ME, Nikolaou E, Blizard A, Pojar S, Howard A, Hyder-Wright A, Devin J, Reiné J, Robinson R,
773 Solórzano C, Jochems S, Kenny-Nyazika T, Ramos-Sevillano E, Weight CM, Myerscough C, McLennan D,
774 MortonB , Gibbons E, Farrar M, Randles V, Burhan H, Chen T, Shandling AD, Campo JJ, Heyderman RS, Gordon
775 SB, Brown JS, Collins AM, Ferreira DM. A Randomised Controlled Trial of Nasal Immunisation with Live
776 Virulence Attenuated Streptococcus pneumoniae Strains using Human Infection Challenge. Medrxiv. 2023.
777 21. Ferreira DM, Neill DR, Bangert M, Gritzfeld JF, Green N, Wright AK, et al. Controlled human infection
778 and rechallenge with Streptococcus pneumoniae reveals the protective efficacy of carriage in healthy adults.
779 Am J Respir Crit Care Med. 2013;187(8):855-64.
780 22. Eshun-Wilson L, Zhang R, Portran D, Nachury MV, Toso DB, Lohr T, et al. Effects of alpha-tubulin
781 acetylation on microtubule structure and stability. Proc Natl Acad Sci U S A. 2019;116(21):10366-71.
782 23. Iliev AI, Djannatian JR, Opazo F, Gerber J, Nau R, Mitchell TJ, et al. Rapid microtubule bundling and
783 stabilization by the Streptococcus pneumoniae neurotoxin pneumolysin in a cholesterol-dependent, non-
784 lytic and Src-kinase dependent manner inhibits intracellular trafficking. Mol Microbiol. 2009;71(2):461-77.
785 24. Surabhi S, Jachmann LH, Shumba P, Burchhardt G, Hammerschmidt S, Siemens N. Hydrogen Peroxide
786 Is Crucial for NLRP3 Inflammasome-Mediated IL-1beta Production and Cell Death in Pneumococcal Infections
787 of Bronchial Epithelial Cells. J Innate Immun. 2022;14(3):192-206.
788 25. Maekawa T, Kashkar H, Coll NS. Dying in self-defence: a comparative overview of immunogenic cell
789 death signalling in animals and plants. Cell Death Differ. 2023;30(2):258-68.
790 26. Gunther C, Buchen B, He GW, Hornef M, Torow N, Neumann H, et al. Caspase-8 controls the gut
791 response to microbial challenges by Tnf-alpha-dependent and independent pathways. Gut. 2015;64(4):601-
792 10.

793 27. Gonzalez-Juarbe N, Bradley KM, Shenoy AT, Gilley RP, Reyes LF, Hinojosa CA, et al. Pore-forming
794 toxin-mediated ion dysregulation leads to death receptor-independent necroptosis of lung epithelial cells
795 during bacterial pneumonia. Cell Death Differ. 2017;24(5):917-28.
796 28. Gonzalez-Juarbe N, Bradley KM, Riegler AN, Reyes LF, Brissac T, Park SS, et al. Bacterial Pore-Forming
797 Toxins Promote the Activation of Caspases in Parallel to Necroptosis to Enhance Alarmin Release and
798 Inflammation During Pneumonia. Sci Rep. 2018;8(1):5846.
799 29. Erttmann SF, Gekara NO. Hydrogen peroxide release by bacteria suppresses inflammasome-
800 dependent innate immunity. Nat Commun. 2019;10(1):3493.
801 30. Alibayov B, Scasny A, Khan F, Creel A, Smith P, Vidal AGJ, et al. Oxidative Reactions Catalyzed by
802 Hydrogen Peroxide Produced by Streptococcus pneumoniae and Other Streptococci Cause the Release and
803 Degradation of Heme from Hemoglobin. Infect Immun. 2022;90(12):e0047122.
804 31. Zafar MA, Wang Y, Hamaguchi S, Weiser JN. Host-to-Host Transmission of Streptococcus pneumoniae
805 Is Driven by Its Inflammatory Toxin, Pneumolysin. Cell Host Microbe. 2017;21(1):73-83.
806 32. Periselneris J, Turner CT, Ercoli G, Szylar G, Weight CM, Thurston T, et al. Pneumolysin suppresses
807 the initial macrophage pro-inflammatory response to Streptococcus pneumoniae. Immunology.
808 2022;167(3):413-27.
809 33. Terra VS, Plumptre CD, Wall EC, Brown JS, Wren BW. Construction of a pneumolysin deficient mutant
810 in streptococcus pneumoniae serotype 1 strain 519/43 and phenotypic characterisation. Microb Pathog.
811 2020;141:103999.
812 34. Bazant J, Ott B, Hudel M, Hain T, Lucas R, Mraheil MA. Impact of Endogenous Pneumococcal
813 Hydrogen Peroxide on the Activity and Release of Pneumolysin. Toxins (Basel). 2023;15(10).
814 35. Travaglini KJ, Nabhan AN, Penland L, Sinha R, Gillich A, Sit RV, et al. A molecular cell atlas of the
815 human lung from single-cell RNA sequencing. Nature. 2020;587(7835):619-25.
816 36. Herta T, Bhattacharyya A, Bollensdorf C, Kabus C, Garcia P, Suttorp N, et al. DNA-release by
817 Streptococcus pneumoniae autolysin LytA induced Krueppel-like factor 4 expression in macrophages. Sci Rep.
818 2018;8(1):5723.
819 37. Barutcu AR, Lajoie BR, Fritz AJ, McCord RP, Nickerson JA, van Wijnen AJ, et al. SMARCA4 regulates
820 gene expression and higher-order chromatin structure in proliferating mammary epithelial cells. Genome
821 Res. 2016;26(9):1188-201.
822 38. Wilson R, Cohen JM, Jose RJ, de Vogel C, Baxendale H, Brown JS. Protection against Streptococcus
823 pneumoniae lung infection after nasopharyngeal colonization requires both humoral and cellular immune
824 responses. Mucosal Immunol. 2015;8(3):627-39.
825 39. Periselneris J, Ercoli G, Pollard T, Chimalapati S, Camberlein E, Szylar G, et al. Relative Contributions
826 of Extracellular and Internalized Bacteria to Early Macrophage Proinflammatory Responses to Streptococcus
827 pneumoniae. mBio. 2019;10(5).
828 40. Belitsky BR, Brill J, Bremer E, Sonenshein AL. Multiple genes for the last step of proline biosynthesis
829 in Bacillus subtilis. J Bacteriol. 2001;183(14):4389-92.
830 41. Sah S, Aluri S, Rex K, Varshney U. One-carbon metabolic pathway rewiring in Escherichia coli reveals
831 an evolutionary advantage of 10-formyltetrahydrofolate synthetase (Fhs) in survival under hypoxia. J
832 Bacteriol. 2015;197(4):717-26.
833 42. Aluri S, Rex K, Varshney U. Simultaneous presence of fhs and purT genes is disadvantageous for the
834 fitness of Escherichia coli growth. FEMS Microbiol Lett. 2015;362(14).
835 43. Obolski U, Swarthout TD, Kalizang'oma A, Mwalukomo TS, Chan JM, Weight CM, et al. The metabolic,
836 virulence and antimicrobial resistance profiles of colonising Streptococcus pneumoniae shift after PCV13
837 introduction in urban Malawi. Nat Commun. 2023;14(1):7477.
838 44. Galan JE. Salmonella Typhimurium and inflammation: a pathogen-centric affair. Nat Rev Microbiol.
839 2021;19(11):716-25.
840 45. Li G, Wang G, Li M, Li L, Liu H, Sun M, et al. Morin inhibits Listeria monocytogenes virulence in vivo
841 and in vitro by targeting listeriolysin O and inflammation. BMC Microbiol. 2020;20(1):112.
842 46. Connor V, German E, Pojar S, Mitsi E, Hales C, Nikolaou E, et al. Hands are vehicles for transmission
843 of Streptococcus pneumoniae in novel controlled human infection study. Eur Respir J. 2018;52(4).
844 47. Lourenco J, Daon Y, Gori A, Obolski U. Pneumococcal Competition Modulates Antibiotic Resistance
845 in the Pre-Vaccination Era: A Modelling Study. Vaccines (Basel). 2021;9(3).

846 48. Watkins ER, Kalizang'Oma A, Gori A, Gupta S, Heyderman RS. Factors affecting antimicrobial
847 resistance in Streptococcus pneumoniae following vaccination introduction. Trends Microbiol.
848 2022;30(12):1135-45.
849 49. Chaguza C, Senghore M, Bojang E, Gladstone RA, Lo SW, Tientcheu PE, et al. Within-host
850 microevolution of Streptococcus pneumoniae is rapid and adaptive during natural colonisation. Nat
851 Commun. 2020;11(1):3442.
852 50. Browall S, Norman M, Tangrot J, Galanis I, Sjostrom K, Dagerhamn J, et al. Intraclonal variations
853 among Streptococcus pneumoniae isolates influence the likelihood of invasive disease in children. J Infect
854 Dis. 2014;209(3):377-88.
855 51. S. A. FastQC: a quality control tool for high throughput sequence data. 2010.
856 52. Ewels P, Magnusson M, Lundin S, Kaller M. MultiQC: summarize analysis results for multiple tools
857 and samples in a single report. Bioinformatics. 2016;32(19):3047-8.
858 53. Bolger AM, Lohse M, Usadel B. Trimmomatic: a flexible trimmer for Illumina sequence data.
859 Bioinformatics. 2014;30(15):2114-20.
860 54. Langmead B, Salzberg SL. Fast gapped-read alignment with Bowtie 2. Nat Methods. 2012;9(4):357-9.
861 55. Li H, Handsaker B, Wysoker A, Fennell T, Ruan J, Homer N, et al. The Sequence Alignment/Map format
862 and SAMtools. Bioinformatics. 2009;25(16):2078-9.
863 56. Nicol JW, Helt GA, Blanchard SG, Jr., Raja A, Loraine AE. The Integrated Genome Browser: free
864 software for distribution and exploration of genome-scale datasets. Bioinformatics. 2009;25(20):2730-1.
865 57. Liao Y, Smyth GK, Shi W. featureCounts: an efficient general purpose program for assigning sequence
866 reads to genomic features. Bioinformatics. 2014;30(7):923-30.
867 58. Love MI, Huber W, Anders S. Moderated estimation of fold change and dispersion for RNA-seq data
868 with DESeq2. Genome Biol. 2014;15(12):550.
869 59. Yu G, Wang LG, Han Y, He QY. clusterProfiler: an R package for comparing biological themes among
870 gene clusters. OMICS. 2012;16(5):284-7.
871 60. Rheinwald JG, Green H. Serial cultivation of strains of human epidermal keratinocytes: the formation
872 of keratinizing colonies from single cells. Cell. 1975;6(3):331-43.
873 61. Carpenter AE, Jones TR, Lamprecht MR, Clarke C, Kang IH, Friman O, et al. CellProfiler: image analysis
874 software for identifying and quantifying cell phenotypes. Genome Biol. 2006;7(10):R100.
875 62. Kirkham LA, Kerr AR, Douce GR, Paterson GK, Dilts DA, Liu DF, et al. Construction and immunological
876 characterization of a novel nontoxic protective pneumolysin mutant for use in future pneumococcal vaccines.
877 Infect Immun. 2006;74(1):586-93.

878

879

880 **SUPPLEMENTAL INFORMATION**

881 ***Streptococcus pneumoniae* with biosynthesis gene mutations that attenuate disease retain**
882 **their potential for epithelial microinvasion and the induction of nasal epithelium innate**
883 **immunity**

884

885 **Table 1. Pneumococcal counts from microscopy nasal curettes.** EHPC raw data for microscopy
886 pneumococcal counts per volunteer. Surface bacteria – association; intracellular – micro-invasion.
887 Microinvasion index (MI) calculated from intracellular bacteria as a percentage of total (intracellular
888 + surface associated) bacteria.

889

890 **Table 2. Differentially upregulated genes by *S. pneumoniae* biosynthesis mutants in**
891 **comparison WT under serum stress.** Enrichment analysis of virulence genes, experimentally
892 deleted biosynthesis genes, purine related genes, hydrogen peroxide regulators and carbohydrate
893 metabolism. A comparison of differential gene expression was assessed when pneumococcal
894 strains were cultured in human serum, comparing the single Δ*proABC* Δ*fhs* mutant relative to the
895 WT strain.

896

897 **Table 3. Primary antibodies used for Microscopy.** Primary and secondary antibodies for epithelial
898 proteins. Primary antibodies were added for 1 hr at room temperature before washing off in HBSS
899 and adding secondary antibodies for 45 minutes.

900

901 **Fig 1. Junctional proteins in Primary HBE-A cells.** Representative example of JAM-A (red, A)
902 and ZO-1 (red, B) staining in primary HBE-A cells after a 6hr infection (green). Nuclei stained with
903 DAPI in blue. Co-localisation of junctional proteins and pneumococci appear yellow, as highlighted
904 by the arrow.

905

906 **Fig 2. Ciliated Primary HBE-A cells.** Representative example of pneumococcal (green)
907 associations with ciliated (acetylated tubulin, red) cells as illustrated with the Δ*proABC+PiaA* mutant
908 in primary HBE-A cells.

909

910 **Fig 3. Association, microinvasion and transmigration of pneumococci following 1hr infection**
911 **in Detroit 562 cells.** Pneumococcal-epithelial interactions at 1hr post infection. Association, micro-
912 invasion and transmigration of pneumococcal strains after 1hr infection in Detroit 562 cells and CFUs
913 recorded. (A) Association of 6B strains. $p = 0.0024$. (B) Internalisation of 6B strains. $p = 0.0107$). (C)
914 Micro-invasive index. Proportion of all bacteria internalised into cells $p = 0.6478$. (D) Transmigration
915 of 6B strains after 1hr infection. Pneumococcal strains were added to the apical chamber of a
916 transwell insert with a confluent monolayer of Detroit 562 cells. CFUs were recorded over time from
917 the basal chamber, reflecting bacteria that had transmigrated across the epithelium. $p = 0.0106$. (E)
918 Pre ($p = 0.5403$) and post ($p = 0.6384$) inoculum. N = 4 independent experiments with replicates
919 (Kruskal-Wallis). (F) Pre and post inoculum after 3 hours infection. Pre- (light grey) and post- (dark
920 grey) inoculums after 3 hours incubation with epithelial cells. Pre- $p = 0.8366$, Post- $p = 0.0160$, 6B
921 v isogenic mutants (Kruskal-Wallis), n = 6 with replicates. (G) Cell supernatant from infected cells

922 was analysed for lactate dehydrogenase secretion. N = 3 - 5 with replicates. p = 0.046 compared to
923 non-infected cells, and p = 0.5649 between 6B WT and mutant strains (ANOVA).

924

925 **Fig 4. Junctional proteins in Detroit 562 cells.** Representative example of junctional protein
926 staining (red) in Detroit 562 cells after 3hr infection (pneumococci green). Nuclei (DAPI, blue). N = 4
927 independent experiments with replicates.

928

Figure 1

A

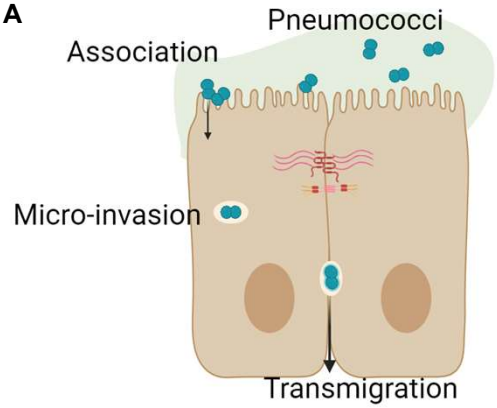

B

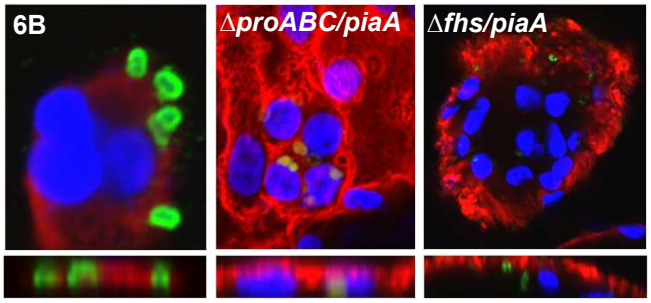

C

	Day 6 post-challenge	
	Association (%)	**Micro-invasion (%)**
6B	87.8 (n11, 43spn)	12.2 (n11, 6spn)
Δ*proABC/piaA*	59.3 (n11, 16spn)	40.7 (n11, 11spn)
Δ*fhs/piaA*	48.7 (n5, 57spn)	51.3 (n5, 60spn)

Figure 2

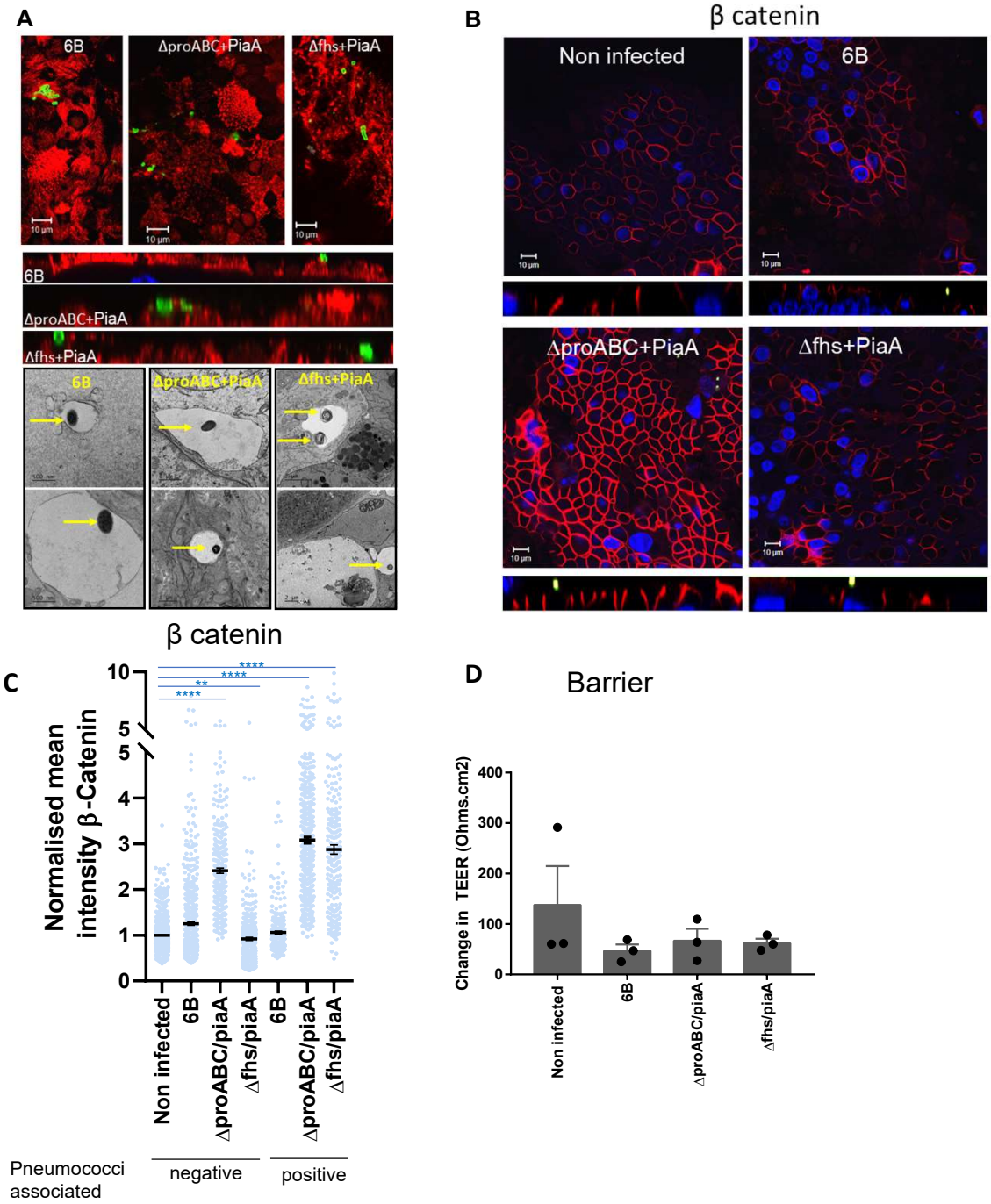
A
6B
ΔproABC+PiaA
Δfhs+PiaA
B
β catenin
Non infected
6B
ΔproABC+PiaA
Δfhs+PiaA
C
β catenin
Normalised mean intensity β-Catenin
Non infected
6B
ΔproABC/piaA
Δfhs/piaA
Pneumococci associated
negative
positive
D
Barrier
Change in TEER (Ohms.cm2)
Non infected
6B
ΔproABC/piaA
Δfhs/piaA

Figure 3

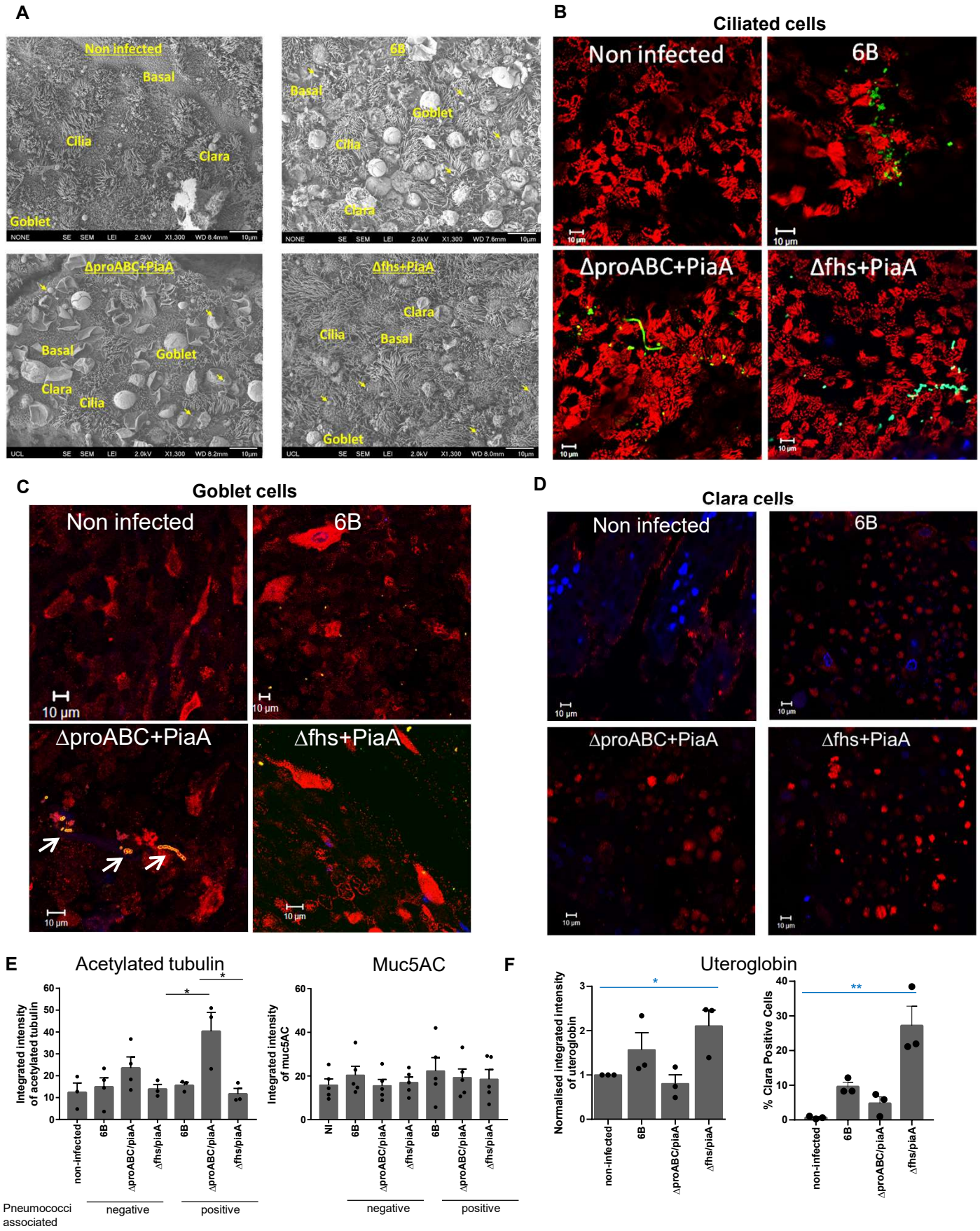
A
Non infected
Basal
Cilia
Clara
Goblet
6B
ΔproABC+PiaA
Δfhs+PiaA
B
Ciliated cells
Non infected
6B
ΔproABC+PiaA
Δfhs+PiaA
C
Goblet cells
Non infected
6B
ΔproABC+PiaA
Δfhs+PiaA
10 µm
D
Clara cells
Non infected
6B
ΔproABC+PiaA
Δfhs+PiaA
E
Acetylated tubulin
Integrated intensity of acetylated tubulin
non-infected
6B
ΔproABC/piaA
Δfhs/piaA
Pneumococci associated
negative
positive
Muc5AC
Integrated intensity of muc5AC
NI
F
Uteroglobin
Normalised integrated intensity of uteroglobin
% Clara Positive Cells

Figure 4

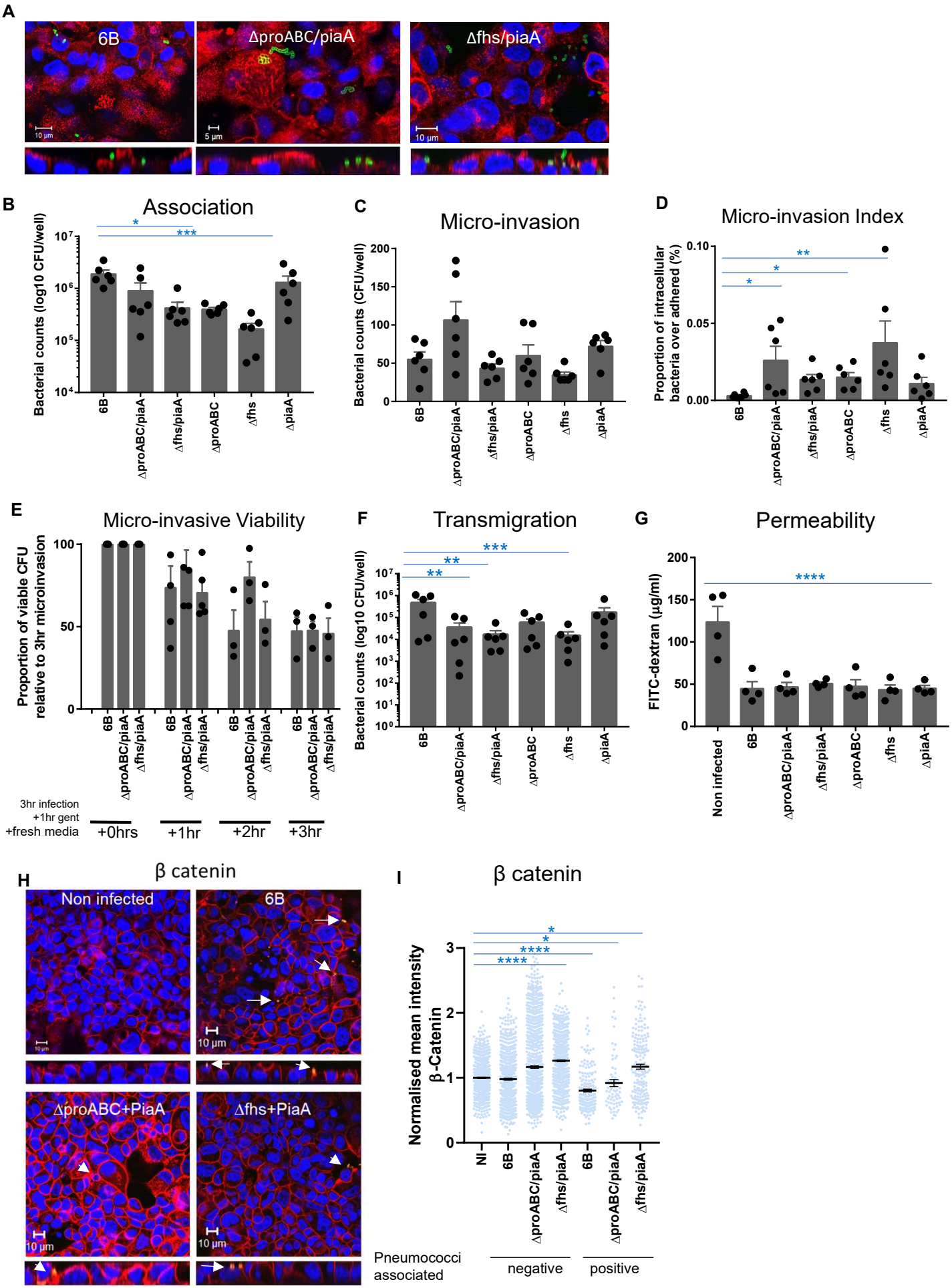
A
6B
ΔproABC/piaA
Δfhs/piaA
10 µm
5 µm
B
Association
Bacterial counts (log10 CFU/well)
6B
ΔproABC/piaA
Δfhs/piaA
ΔproABC
Δfhs
ΔpiaA
C
Micro-invasion
Bacterial counts (CFU/well)
D
Micro-invasion Index
Proportion of intracellular bacteria over adhered (%)
E
Micro-invasive Viability
Proportion of viable CFU relative to 3hr microinvasion
3hr infection
+1hr gent
+fresh media
+0hrs
+1hr
+2hr
+3hr
F
Transmigration
Bacterial counts (log10 CFU/well)
G
Permeability
FITC-dextran (µg/ml)
Non infected
H
β catenin
Non infected
6B
ΔproABC+PiaA
Δfhs+PiaA
I
β catenin
Normalised mean intensity β-Catenin
NI
Pneumococci associated
negative
positive

Figure 5

A

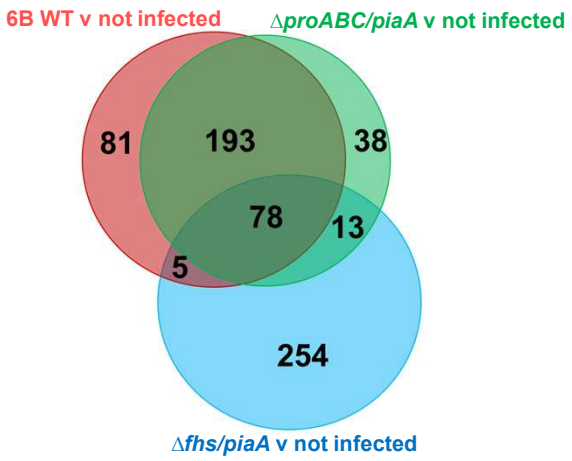

B

log2foldchange	6B	ΔproABC/piaA	Δfhs/piaA
Upregulated genes			
AC256236.1	32.9	25.5	0.0
AC022149.1	30.2	27.6	0.0
Z84488.2	29.1	21.6	0.0
MUC21	25.8	29.0	0.0
VASN	20.9	0.0	0.0
BRD2	18.4	24.7	0.0
AC012254.2	18.2	13.8	0.0
CTAGE4	18.1	0.0	0.0
MICE	17.1	20.3	0.0
AC107075.1	10.1	0.0	0.0
CSNK2B	0.0	20.2	0.0
MTRNR2L6	0.0	19.4	15.8
LSM2	0.0	17.1	0.0
ALOX5	0.0	0.0	6.9
AC006064.6	0.0	0.0	3.4
TAP2	0.0	0.0	3.2
CYP1A1	0.0	0.0	1.7
FOSB	0.0	0.0	1.4
IL1B	0.0	0.0	1.3
CXCL8	0.0	0.0	1.1
CXCL2	0.0	0.0	1.1
CYP1B1	0.0	0.0	1.0

C

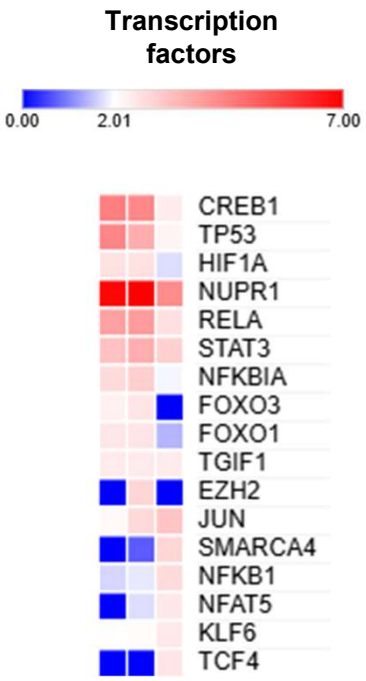

D

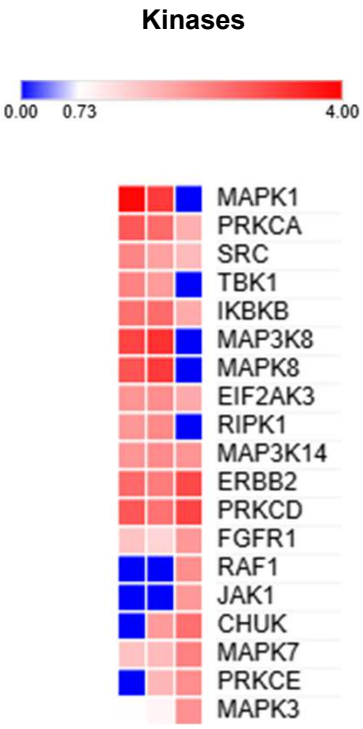

Figure 6

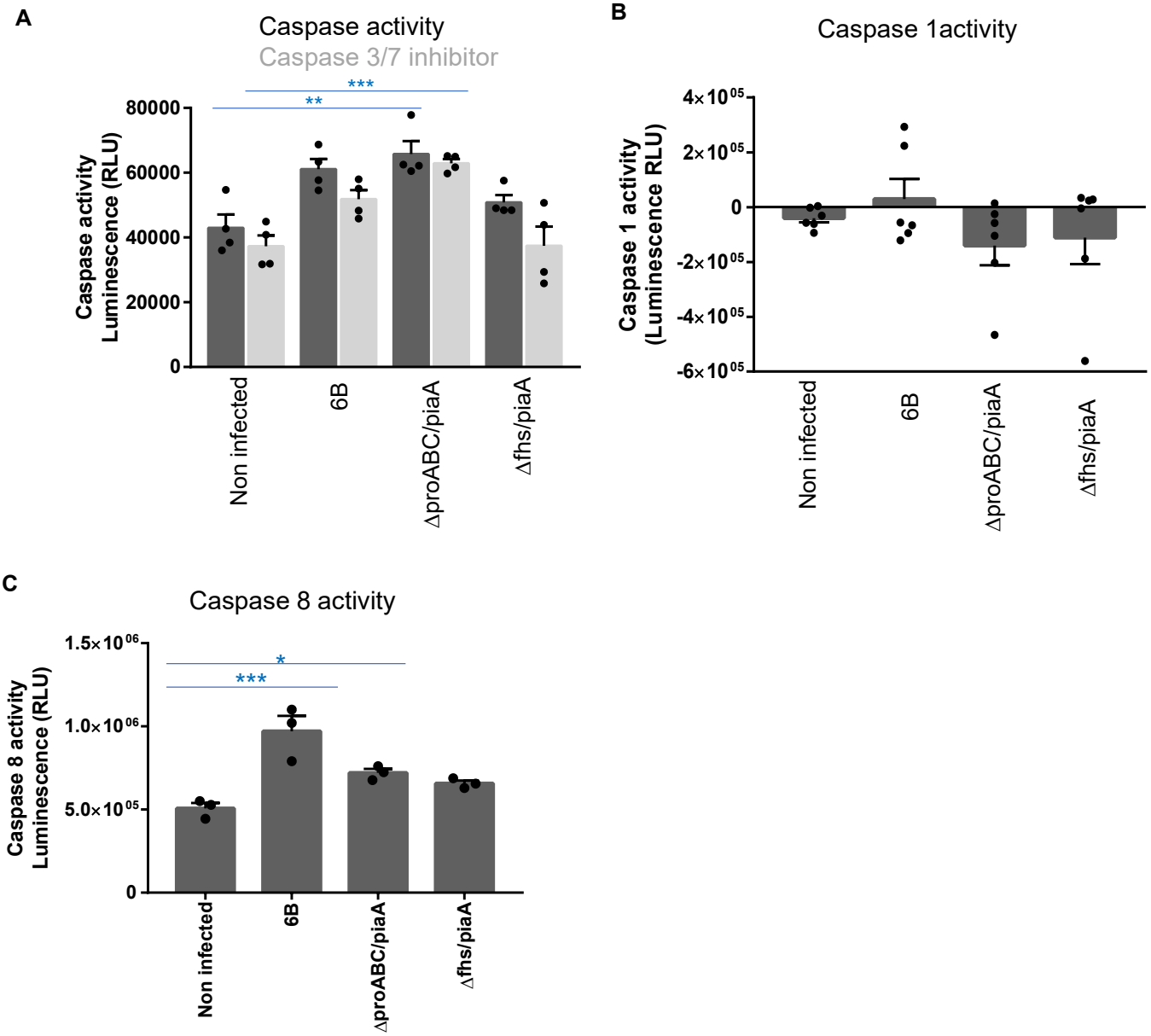
A
Caspase activity
Caspase 3/7 inhibitor
Caspase activity
Luminescence (RLU)
80000
60000
40000
20000
0
***
**
Non infected
6B
ΔproABC/piaA
Δfhs/piaA
B
Caspase 1activity
Caspase 1 activity
(Luminescence RLU)
4×10^05
2×10^05
0
-2×10^05
-4×10^05
-6×10^05
Non infected
6B
ΔproABC/piaA
Δfhs/piaA
C
Caspase 8 activity
Caspase 8 activity
Luminescence (RLU)
1.5×10^06
1.0×10^06
5.0×10^05
0
*
***
Non infected
6B
ΔproABC/piaA
Δfhs/piaA

Figure 7

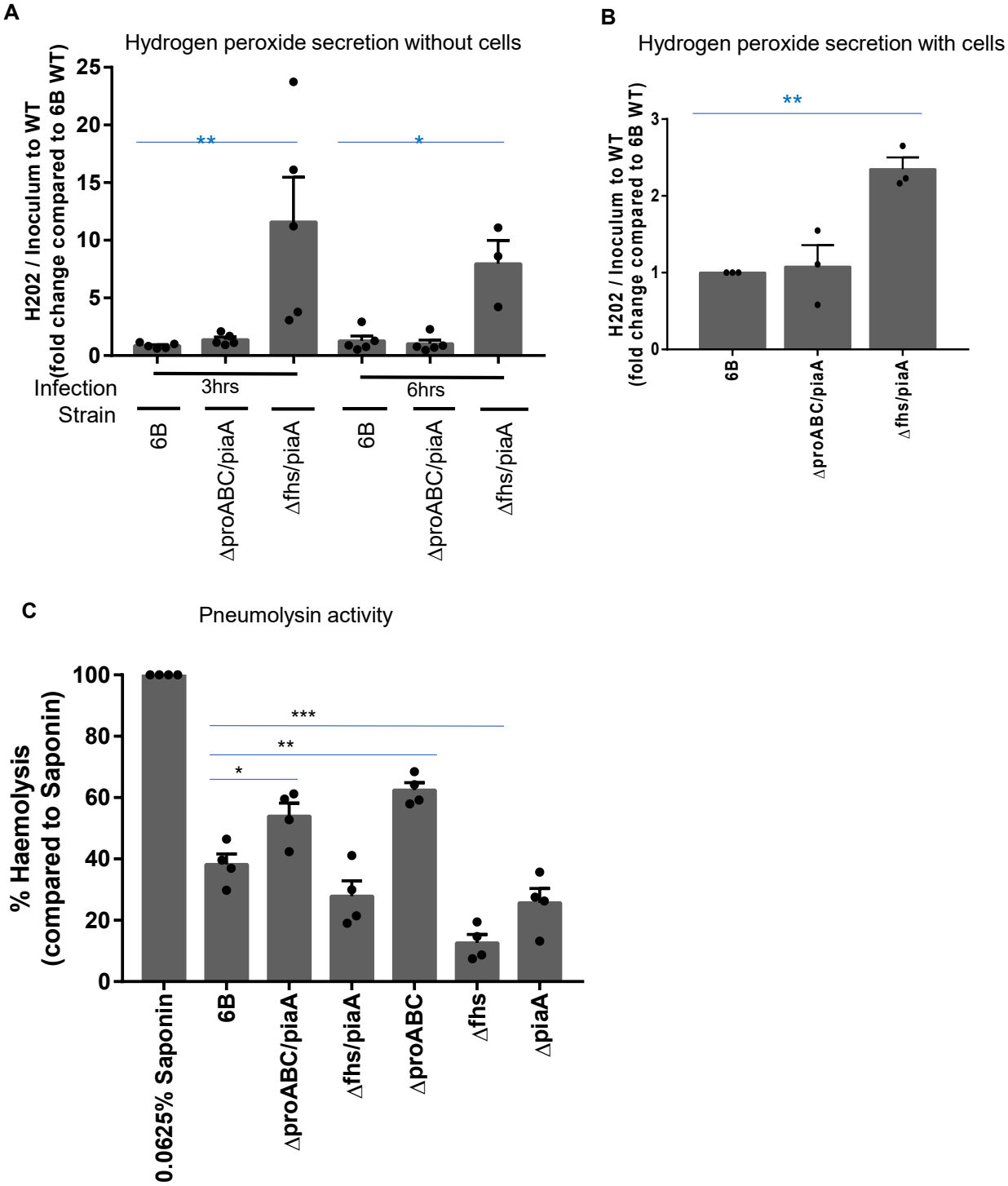
A
Hydrogen peroxide secretion without cells
H202 / Inoculum to WT
(fold change compared to 6B WT)
25
20
15
10
5
0
**
*
Infection
3hrs
6hrs
Strain
6B
ΔproABC/piaA
Δfhs/piaA
6B
ΔproABC/piaA
Δfhs/piaA
B
Hydrogen peroxide secretion with cells
H202 / Inoculum to WT
(fold change compared to 6B WT)
3
2
1
0
**
6B
ΔproABC/piaA
Δfhs/piaA
C
Pneumolysin activity
% Haemolysis
(compared to Saponin)
100
80
60
40
20
0
***
**
*
0.0625% Saponin
6B
ΔproABC/piaA
Δfhs/piaA
ΔproABC
Δfhs
ΔpiaA
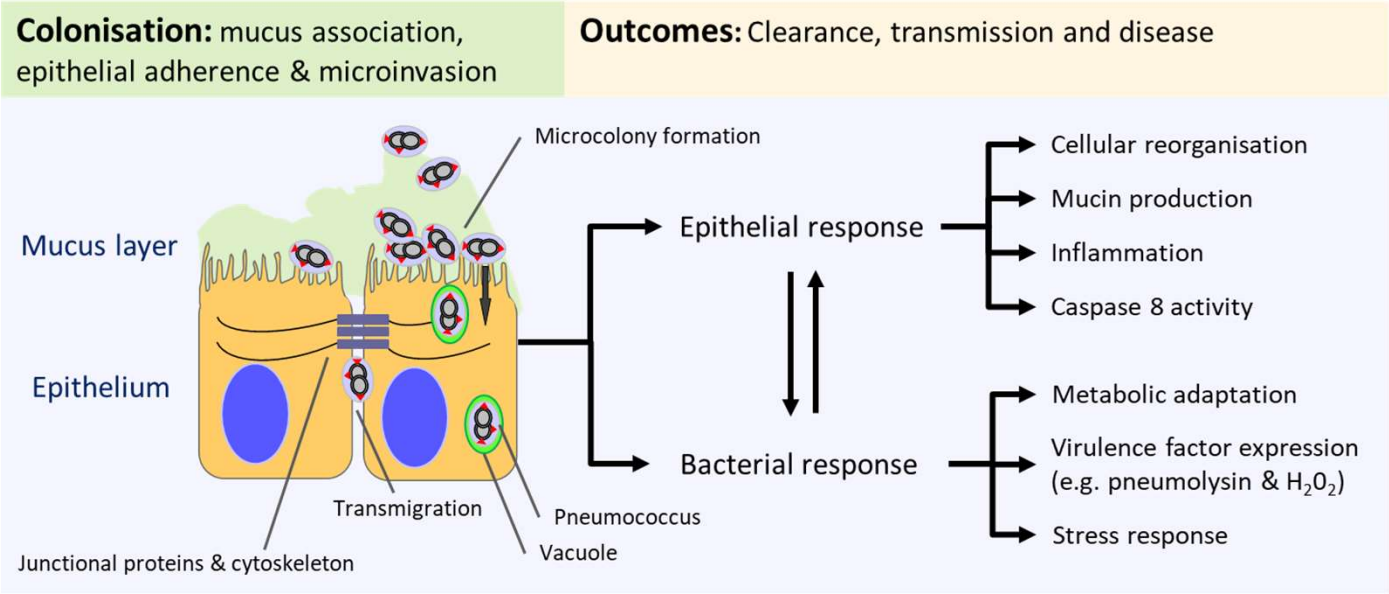
Graphical abstract